Research on Stabilizing and Eliminating Limit Cycles in 3D Nonlinear Systems Characterized by Hysteresis

KARTIK CHANDRA PATRA[1*], ASUTOSH PATNAIK[2]
[1, 2] Department of Electrical Engineering
C. V. Raman Global University, Bhubaneswar, Odisha 752054, INDIA
Corresponding Author
ORCID ID: 0000-0002-4693-4883

Abstract: -The work proposes a systematic and innovative graphical technique that practices computer graphics in the prediction of limit cycles (LC) in 3×3 multivariable systems with memory-type nonlinearities. If the system in an autonomous state exhibits LC, the present work investigates the quenching of LC using the method of signal stabilization with high-frequency signals random/deterministic. State feedback combined with pole placement techniques is a key strategy for suppression of LC oscillations. The feedback gain K is determined either through arbitrary selection of poles, subject to controllability conditions, or optimally, using the Riccati equation. The complexity involved in formulating the problem with memory-type nonlinearities is reduced considerably using the harmonic linearization. The complexity is further reduced if the system considered shows the LC primarily at a single frequency. The proposed methods are illustrated using examples and validation, done by digital simulation and by using SIMULINK Toolbox of MATLAB software.

Keywords: Limit Cycles; Describing function; Signal stabilization; Pole Placement; 3×3 Nonlinear Systems; Rectangular Hysteresis Type Nonlinearities; Backlash Nonlinearities;

Received: February 17, 2025. Revised: September 6, 2025. Accepted: September 12, 2025. Published: November 1, 2025.

1 Introduction

For decades, researchers have been increasingly focused on the prediction of limit cycles (LC) in 2×2 nonlinear systems, in fact demonstrated by a thorough literature survey in [1-40]. The problem is more notable and acute in the memory type of nonlinearity, which has been addressed to a certain extent in [41-43]. Until [5, 38] almost no literature is available that addresses the quenching of LC. The scarcity of literature on quenching self-sustained oscillations in autonomous 2×2 nonlinear systems exacerbates the problem in [5, 38].

However, there is little literature available that addresses 3×3 nonlinear systems and discusses limit cycles and their quenching/suppression. The available papers [30-33, 42, 44] have attempted to focus their research in this area but are confined to non-memory type nonlinearity in 3-dimensional case. It is seen and apparent that in 3×3 nonlinear systems LC exhibits in several cases, like the boiler turbine unit. A 3×3 system that shows nonlinear dynamics in a wide range of operations is cited in [30]. Several other chemical processes are multi-dimensional and consider a 3×3 model where LC has been reported as in [33]. Similarly, a good number of problems related to industries with two- or higher-dimensional configurations are cited in [11].

The describing function (DF) method is absolutely essential for prediction of LC, which has been stated in [4, 5, 10, 11, 13, 20, 45]. Investigation/prediction of LC in 3×3 nonlinear systems compatible with the structure of general 3×3 systems as in [46] caught the attention and is presented in this paper. The mathematical formulation of the problem analytically following the suggested structure is quite complex and involved, in particular with memory-type nonlinearities, even by use of harmonic balance as cited in [40]. Hence, in the present work a graphical method has been developed for investigation of LC in 3×3 systems with memory-type nonlinearities.

The most common nonlinearity is backlash, which occurs frequently in physical systems, causing LC that acts as a constraint on speed and position control performance in the robotics and automation industry and has been extensively discussed in multivariable systems such as [26, 27, 31, 34-40]. The backlash is an inherent characteristic of the governor that affects the performance in load frequency control with multi-area power systems due to the exhibition of LC cited in [31, 43].

The proposed work is presented in the following sequences. Section 2 is a graphical technique developed for exploration of LC in 3-dimensional

DOI: 10.37394/232026.2025.7.19

nonlinear systems with memory-type nonlinearities, which is an extension/advancement presented in [46] and also the steps stated in [38]. Section 3 is the signal stabilization, which illustrates the procedure through memory-type nonlinearities using deterministic/random (Gaussian) signals. Section 4 depicts the suppression of LC applying the pole placement method with a suitable state feedback gain matrix K determined either through arbitrary selection of poles, subject to complete controllability conditions, or determined optimally using the Riccati equation.

Section 3 analyzes system dynamics represented in a class 3x3 multivariable system as in Figure 1. For the autonomous case (U=0), the governing equation under LC conditions, expressed in the frequency domain, is C = GN(X)X and X = -HC. This leads to X = AX = -HGN(X)X =, where A = -HGN(X) in [40], facilitating eigenvalue calculation in Section 2.1 of [44]. X_i and C_i represent the amplitudes of the sinusoids and the corresponding outputs, respectively. G_i and N_i are the magnitudes of the associated functions (i = 1, 2, 3).

It is worthy to note that in frequency response analysis, the input is a sinusoid and the output is considered at steady-state. This allows for the substitution of the Laplace operator, s, with jω.

2. Investigation of LC in 3×3 Systems Subject to Memory-Based Nonlinearities

2.1 Graphical Method

Considering the complexity and many involved mathematical derivations, a graphical method [44, 46] has been opted for investigation of LC in 3×3 nonlinear systems. Consider a system having three interconnected systems as given in Figure 1. In the system N_1, N_2 & N_3 are 3 nonlinear elements with rectangular hysteresis-type input/output characteristics as revealed in Figures 2(a), 2(b), and 2(c), respectively. $G_1(s)$, $G_2(s)$, and $G_3(s)$ are transfer functions of three linear elements.

The graphical technique based on a normalized phasor diagram similar to that in [40] is developed in a 3×3 system for investigation of LC in the system, which has been shown through Examples 1 and 2. The analysis assumes that the system shows self-sustained oscillation predominantly at a particular frequency.

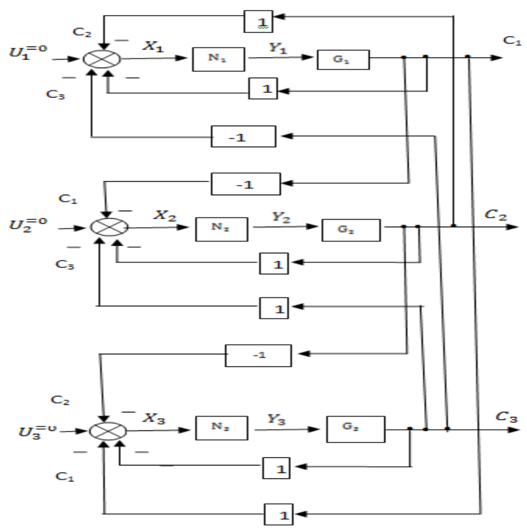

Fig. 1: A class of 3×3 multivariable nonlinear systems

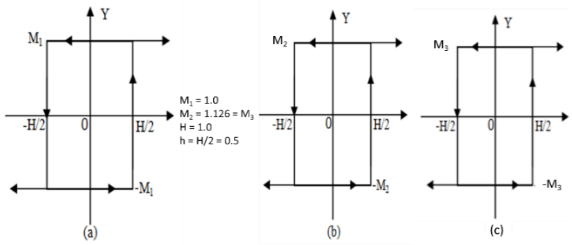

Fig. 2: Rectangular Hysteresis Characteristics of nonlinear elements N_1, N_2, and N_3

The rectangular hysteresis characteristics contribute an additional phase loop angle to the loop phase angle generated by $G_1(j\omega)$, $G_2(j\omega)$, and $G_3(j\omega)$, the transfer functions (TFs) of the subsystems S_1, S_2 and S_3. By substituting the nonlinear elements with their corresponding DFs and applying the principle of harmonic balance, the existence of limit cycles is contingent upon three specific conditions [46]. The first of these conditions, applicable to memory-type nonlinearities:

(i) The phase of the loop should be $\theta = 180^o = \angle G_1 + \angle G_2 + \angle G_3 + \angle N_1 + \angle N_2 + \angle N_3$: where loop angle of G and phase shift of N, corresponding DFs.

(ii) The Gain condition: $\frac{C_1}{R_1} \times \frac{C_2}{R_2} \times \frac{C_3}{R_3} = 1$: where, $\frac{C_1}{R_1} = \frac{G_1(j\omega)N_1(X_{m1},\omega)}{1+G_1(j\omega)N_1(X_{m1},\omega)}$; $\frac{C_2}{R_2} = \frac{G_2(j\omega)N_2(X_{m2},\omega)}{1+G_2(j\omega)N_2(X_{m2},\omega)}$; $\frac{C_3}{R_3} = \frac{G_3(j\omega)N_3(X_{m3},\omega)}{1+G_3(j\omega)N_3(X_{m3},\omega)}$

(iii) The Amplitude Ratio condition: $\frac{X_1}{X_2} = \frac{V_1}{V_2}$; $\frac{X_2}{X_3} = \frac{V_2}{V_3}$; $\frac{X_3}{X_1} = \frac{V_3}{V_1}$: where $X_1 = X_{m1}$; $X_2 = X_{m2}$; $X_3 = X_{m3}$ and V_1, V_2, and V_3 are the Eigen vectors.

2.1.1 Example 1

Consider the system of Figure 2 with $G_1(s) = \frac{2}{s(s+1)^2}$; $G_2(s) = \frac{1}{s(s+4)}$; $G_3(s) = \frac{1}{s(s+2)}$ and the three nonlinear functions having rectangular hysteresis characteristics having $M_1 = 1.0$, $M_2 = M_3 = 1.126$ and $H = 1.0$, $h = H/2 = 0.5$ as shown in Figures 3(a), 3(b), and 3(c).

The DF for a rectangular hysteresis nonlinearity is given by:

$$N(X_m, \omega) = \left|\frac{Y}{Xm} < \phi\right| = 0\ ,\ X < \frac{H}{2} \quad \ldots. \quad (1)$$

$$\frac{4M}{\emptyset X} < -\sin^{-1}\frac{H}{2X}, \quad X > \frac{H}{2}$$

This is expanded in $(a + jb)$ forms (c f Eqns. 2, 4, and 6)

$$N_1(X_1, \omega_1) = \frac{4M_1}{\pi X_1}\left[\cos\left(sin^{-1}\frac{1}{2X_1}\right) - j\frac{1}{2X_1}\right] \quad \ldots\ldots \quad (2)$$

$$N_1{}'(X_1, \omega_1) = \frac{-4M_1}{\pi X_1^2}\cos\left(sin^{-1}\frac{1}{2X_1}\right) + \frac{2}{\pi X_1^4} \times \frac{1}{\sqrt{1-(1/4X_1)}} + j\frac{4M_1}{\pi X_1^3} \quad \ldots\ldots \quad (3)$$

$$N_2(X_2, \omega_2) = \frac{4M_2}{\pi X_2}\left[\cos\left(sin^{-1}\frac{1}{2X_2}\right) - j\frac{1}{2X_2}\right] \quad \ldots \quad (4)$$

$$N_2{}'(X_2, \omega_2) = \frac{-4M_2}{\pi X_2^2}\cos\left(sin^{-1}\frac{1}{2X_2}\right) + \frac{2}{\pi X_2^4} \times \frac{1}{\sqrt{1-(1/4X_2)}} + j\frac{4M_2}{\pi X_2^3} \quad \ldots\ldots \quad (5)$$

$$N_3(X_3, \omega_3) = \frac{4M_3}{\pi X_3}\left[\cos\left(sin^{-1}\frac{1}{2X_3}\right) - j\frac{1}{2X_3}\right] \quad \ldots \quad (6)$$

$$N_3{}'(X_3, \omega_3) = \frac{-4M_3}{\pi X_3^2}\cos\left(sin^{-1}\frac{1}{2X_3}\right) + \frac{2}{\pi X_3^4} \times \frac{1}{\sqrt{1-(1/4X_3)}} + j\frac{4M_3}{\pi X_3^3} \quad \ldots\ldots\ldots\ldots \quad (7)$$

The Newton-Raphson (NR) method was employed to solve Equations (2), (4), and (6). Although phase angles were not directly used during the iterative solution process, they were subsequently included in the loop angle calculations, as shown in Equations (8), (9), and (10). However, the phase angle condition (c f Eqn. (i): phase $\theta = 180^o = \angle G_1 + \angle G_2 + \angle G_3 + \angle N_1 + \angle N_2 + \angle N_3$:was checked at every iteration step. Normalized phase diagrams were constructed for three distinct sets:

Set 1: Subsystems S1, S2, and S3; C1 (-), C2 (-), C3 (+) (Figure 3a)

Set 2: Subsystems S2, S3, and S1; C2 (-), C3 (-), C1 (+) (Figure 3b)

Set 3: Subsystems S1, S3, and S2; C3 (-), C1 (-), C2 (+) (Figure 3c)

For subsystem (S_1)

$$\theta_{L_1} = \theta_{N_1(X_1,\omega)} + \theta_{G_1(j\omega)}$$

$$\theta_{L_1} = -\sin^{-1}\frac{H}{2X_1} - \frac{\pi}{2} - 2\tan^{-1}\omega \quad \ldots\ldots \quad (8)$$

For subsystem (S_2)

$$\theta_{L_2} = \theta_{N_2(X_2,\omega)} + \theta_{G_2(j\omega)}$$

$$\text{or}\ \theta_{L_2} = -\sin^{-1}\frac{H}{2X_2} - \frac{\pi}{2} - \tan^{-1}\frac{\omega}{4} \quad \ldots\ldots \quad (9)$$

For subsystem (S_3)

$$\theta_{L_3} = \theta_{N_3(X_3,\omega)} + \theta_{G_3(j\omega)}$$

$$\text{or}\ \theta_{L_3} = -\sin^{-1}\frac{H}{2X_3} - \frac{\pi}{2} - \tan^{-1}\frac{\omega}{2} \ldots.. \quad (10)$$

In the graphical method while θ_{L_1} traces a circle, θ_{L_2} traces a straight line, and θ_{L_3} traces a straight line from opposite side of θ_{L_2} straight line. Radius of the circle is:

$r = \frac{1}{2\sin\theta_{L_1}}$, and the centre is at

$$\left(0.5, \frac{-1}{2\tan\theta_{L_1}}\right) \ldots\ldots (11)$$

The point where the circle and st. line intersect is located at (u_i, v_i), and is found using the following method:

$$u_i = \frac{v_i}{\tan\theta_{L_2}} - 1 \qquad \ldots.(12)$$

$$\text{And } v_i = \frac{3\cot\theta_{L_2} + \cot\theta_{L_1} \pm \sqrt{(3\cot\theta_{L_2} + \cot\theta_{L_1})^2 - 8csc^2\theta_{L_2}}}{2csc^2\theta_{L_2}} \ldots (13)$$

With ω held constant, the normalized phase diagrams for the three subsystem sets are presented in Figures 3(a), (b), and (c). The analysis of limit cycle conditions and related quantities can be determined using any of these sets.

$$N_2 = (11-3\omega^2)\omega^2 \pm \sqrt{(11-3\omega^2)\omega^4 - 8(\omega^2+16)(1-\omega^2)^2\omega^2} \quad (14),$$

$$N_1 = \frac{(\omega^2-1)}{8}N_2 + \frac{9\omega^2-\omega^4}{8} \quad \cdots (15),$$

$$\frac{Xm_1}{Xm_2} = \frac{X_1}{X_2} = \frac{(1+\omega^2)\sqrt{[\omega^2(\omega^2+16-2N_2)+N_2^2]}}{2N_1\sqrt{\omega^2+16}} \quad \cdots (16),$$

$$\frac{X_1}{X_2} = \frac{BD_i}{AD_i} = \sqrt{\frac{(1-u_i)^2+(u_i)^2}{(1+u_i)^2+(u_i)^2}} \quad \cdots (17),$$

$\Theta L_1 = \theta N_1(Xm_1, \omega) + \theta G_1$, $\Theta L_2 = \theta N_2(Xm_2, \omega) + \theta G_2$, $\Theta L_3 = \theta N_3(Xm_3, \omega) + \theta G_3$, $r_1 = \frac{1}{2\,sin\,\Theta L_1}$ and Centre $C\left(\frac{1}{2}, -\frac{1}{2\,tan\,\Theta L_1}\right)$

For set 1:

$\theta_{L_1} = -\sin^{-1}\frac{H}{2X_1} - \frac{\pi}{2} - 2\tan^{-1}\omega$; $\theta_{L_2} = -\sin^{-1}\frac{H}{2X_2} - \frac{\pi}{2} - \tan^{-1}\frac{\omega}{4}$; $\theta_{L_3} = -\sin^{-1}\frac{H}{2X_3} - \frac{\pi}{2} - \tan^{-1}\frac{\omega}{2}$

DOI: 10.37394/232026.2025.7.19

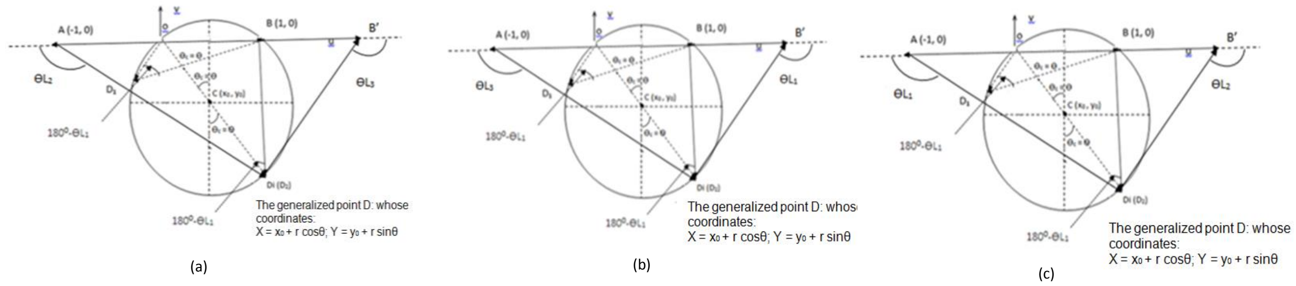

Fig. 3: represents the (a) Normalised Phase Diagram with C_1, C_2 & C_3 for the set 1, where C_1 (-), C_2 (-) and C_3 (+). (b): Normalised Phase Diagram with C_1, C_2 & C_3 for the set 2, where C_2 (-), C_3 (-) and C_1 (+). (c): Normalised Phase Diagram with C_1, C_2 & C_3 for the set 3, C_3 (-), C_1 (-) and C_2 (+).

Table 1: shows the θL_1, θL_2, θL_3, radius (r), centre of the circle, and the intersection points between the two straight lines and the circle for sets 1,2, and 3 representing the example 1.

Table 1a: Numerical Values of Quantities of Example 1 (Rectangular Hysteresis) for set 1

ω	N_1	N_2	N_3	X_{m1}	X_{m2}	X_{m3}	θ_{L1}	θ_{L2}	θ_{L3}	Radius r	Centre $(\mathbf{0.5}, \frac{-1}{2\tan\theta_{L_1}})$
0.60	0.3524	0.4547	0.4547	3.1528	3.6128	3.6128	-161.0	-106.4	-114.6	1.58	0.5, -1.46
0.61	0.3647	0.4662	0.4662	3.0750	3.4911	3.4911	-162.1	-106.9	-115.2	1.63	0.5, -1.55
0.62	0.3772	0.4779	0.4779	2.9997	3.3755	3.3755	-163.1	-107.3	-115.7	1.73	0.5, -1.66
0.63	**0.3899**	**0.4898**	**0.4898**	**2.9269**	**3.2656**	**3.2656**	**-164.1**	**-107.7**	**-116.2**	**1.83**	**0.5, -1.76**
0.64	0.4028	0.5019	0.5019	2.8564	3.1611	3.1611	-166.3	-108.1	-116.8	2.11	0.5, -2.05
0.65	0.4159	0.5142	0.5142	2.7881	3.0600	3.0600	-166.3	-108.6	-117.4	2.12	0.5, -2.06
0.70	0.4843	0.5788	0.5788	2.4771	2.6288	2.6288	-171.6	-110.8	-120.2	3.47	0.5, -3.40

Table 1b: Phase Diagrams Constructed Graphically of Example 1 (Rectangular Hysteresis) with varying ω and corresponding r for set 1

ω	Radius r	Centre $\left(0.5, \dfrac{-1}{2\tan\theta_{L_1}}\right)$	$\dfrac{X_1}{X_2} = \dfrac{BD'}{AD'}$ From plot	$\dfrac{X_1}{X_2} = \dfrac{Xm_1}{Xm_2}$ From Table 1a	$\dfrac{X_1}{X_3} = \dfrac{BD'}{B'D'}$ from plot	$\dfrac{Xm_1}{Xm_3}$ From the Table 1a	Phasor Diagram
0.60	1.58	0.5, -1.46		0.87		0.87	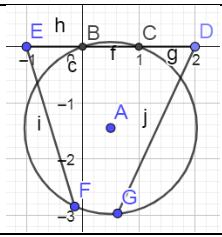
0.63	**1.83**	**0.5, -1.76**	**0.97**	**0.90**	**0.91**	**0.90 (result matched with the plot)**	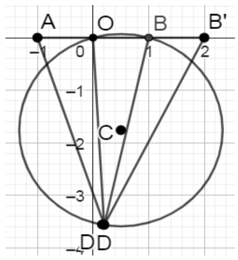 **OD′ = 3.57 = C_1/R_1 = C_1** **OA = 1 = C_2** **BB′ = 1= C_3** **BD′ = 3.65 = X_1** **AD′ = 3.76 = X_2** **B′D′=3.99 = X_3** **X_1/X_2 = BD′/AD′ = 0.97** **X_1/X_3 = BD′/B′D′ = 0.91**
0.64	2.11	0.5, -2.05		0.90		0.90	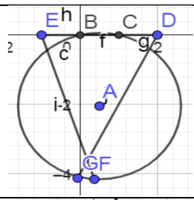
0.65	2.12	0.5, -2.06		0.91		0.91	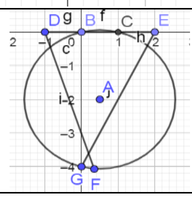

The data presented in Table 1 contain the measurements of $\frac{X1}{X2}$ for different ω using Eqn. (16) as well as the graphical plots of normalised phase diagrams. When $\frac{X1}{X2}$ is calculated from Eqn. (16), it matches with $\frac{X1}{X2}$ obtained from the graphical plot (**BD'/AD'**), confirming the limit cycling condition. Or $\frac{X1}{X3}$ calculated from Table 1a matches with $\frac{X1}{X3}$ obtained from graphical plot (**BD'/B'D'**), confirming the LC condition.

Table 1 (a): Shows **ω, N_1, N_2, N_3, X_{m1}, X_{m2}, X_{m3},** θL_1, θL_2, θL_3, r (radius), and centre of the circle for set 1 of example 1 (rectangular hysteresis).

Table 1 (b): Shows **ω,** r (radius) and centre of the circle for set 1 for example 1 (rectangular hysteresis), $\frac{X_1}{X_2}$ from Table 1a and $\frac{X_1}{X_2} = \frac{\mathbf{BD'}}{\mathbf{AD'}}$ from plot. Or $\frac{Xm1}{Xm3} = \frac{X1}{X3}$ from Table 1a and $\frac{X1}{X3} = \mathbf{BD'/B'D'}$

2.1.2 Example: 2

The system under consideration, presented in Figure 1, has $G_1(s) = \frac{2}{s(s+1)^2}$; $G_2(s) = \frac{1}{s(s+4)}$; $G_3(s) = \frac{1}{s(s+2)}$ and the three nonlinear elements having backlash characteristics with $b_1 = b_2 = b_3 = 1.0$, as shown in Figures 4(a), 4(b), and 4(c).

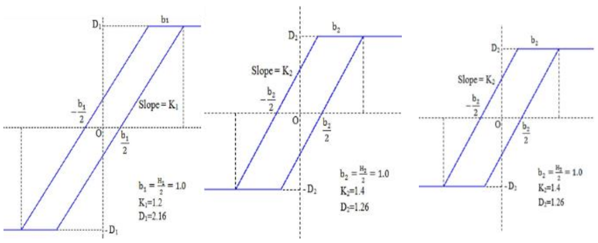

(a) (b) (c)

Fig. 4: Input and output characteristics of nonlinear elements, N_1, N_2, and N_3.

DF of the above backlash nonlinearities is expressed as:

$$N(Xm,\omega) = \left\{\frac{K}{\pi}\sqrt{(\frac{\pi}{2}+\beta+\frac{1}{2}sin2\,\beta)^2+\cos^4\beta}\right\}\angle - \tan^{-1}\left(\frac{\cos^2\beta}{\frac{\pi}{2}+\beta+\frac{1}{2}sin2\,\beta}\right) \quad \text{for } X\,m > \frac{b}{2} \cdots \cdots (18)$$

$$= 0 \quad for\ X_m < \frac{b}{2}$$

And

$$N_1(\mathrm{Xm},\omega) = \frac{K_1}{\pi}\sqrt{(\frac{\pi}{2}+\beta_1+\frac{1}{2}sin2\,\beta_1)^2+\cos^4\beta_1} \quad \ldots(19)\ \ and$$

$$N_2(\mathrm{Xm}_2,\omega) = \frac{K_2}{\pi}\sqrt{(\frac{\pi}{2}+\beta_2+\frac{1}{2}sin2\,\beta_2)^2+\cos^4\beta_2} \quad \ldots(20)\ \ and$$

$$N_3(\mathrm{Xm}_3,\omega) = \frac{K_3}{\pi}\sqrt{(\frac{\pi}{2}+\beta_3+\frac{1}{2}sin2\,\beta_3)^2+\cos^4\beta_3} \quad \ldots\ (21)$$

The derivative of the DF is calculated as:

$$N_1{}'(X_{m1},\omega) = \frac{K_1}{\pi}\times\frac{1}{\sqrt{(\frac{\pi}{2}+\beta_1+{}^1\!/_2\sin 2\,\beta_1)^2+cos^4\beta_1}}\times \left(2\times\left(\frac{\pi}{2}+\beta_1+\frac{1}{2}\sin 2\,\beta_1\right)+(1+\cos 2\beta_1)+2\times(\cos 2\beta_1+1)\times(-2sin^2\beta_1)\right) \quad \ldots \quad (22)$$

$$f_1(X_{m1}) = \frac{K_1}{\pi}\sqrt{(\frac{\pi}{2}+\beta_1+{}^1\!/_2\sin 2\,\beta_1)^2+cos^4\beta_1} - N_1(X_{m1}) \quad \ldots \quad (23)$$

$$f_1{}'(X_{m1}) = \frac{K_1}{\pi}\times\frac{1}{\sqrt{(\frac{\pi}{2}+\beta_1+{}^1\!/_2\sin 2\,\beta_1)^2+cos^4\beta_1}}\times \left(2\times\left(\frac{\pi}{2}+\beta_1+\frac{1}{2}\sin 2\,\beta_1\right)+(1+\cos 2\beta_1)+2\times(\cos 2\beta_1+1)\times(-2sin^2\beta_1)\right) N_1{}'(X_{m1}) \quad \ldots\ (24)$$

Again,

$$N_2(X_{m2},\omega) = \frac{K_2}{\pi}\sqrt{(\frac{\pi}{2}+\beta_2+{}^1\!/_2\sin 2\,\beta_2)^2+cos^4\beta_2} \quad \ldots \quad (25)$$

The derivative of the DF is calculated as:

$$N_2{}'(X_{m2},\omega) = \frac{K_2}{\pi}\times\frac{1}{\sqrt{(\frac{\pi}{2}+\beta_2+{}^1\!/_2\sin 2\,\beta_2)^2+cos^4\beta_2}}\times \left(2\times\left(\frac{\pi}{2}+\beta_2+\frac{1}{2}\sin 2\,\beta_2\right)+(1+\cos 2\beta_2)+2\times(\cos 2\beta_2+1)\times(-2sin^2\beta_2)\right) \quad \ldots (26)$$

$$f_2(X_{m2}) = \frac{K_2}{\pi}\sqrt{(\frac{\pi}{2}+\beta_2+{}^1\!/_2\sin 2\,\beta_2)^2+cos^4\beta_2} - N_2(X_{m2}) \quad \ldots \quad (27)$$

$$f_2{}'(X_{m2}) = \frac{K_1}{\pi}\times\frac{1}{\sqrt{(\frac{\pi}{2}+\beta_2+{}^1\!/_2\sin 2\,\beta_2)^2+cos^4\beta_2}}\times\left(2\left(\frac{\pi}{2}+\beta_2+\frac{1}{2}\sin 2\,\beta_2\right)+(1+\cos 2\beta_2)+\ 2(\cos 2\beta_2+1)\times(-2sin^2\beta_2)\right) - N_1{}'(X_{m1}) \quad \ldots \quad (28)$$

Because the relationships between N_1 and X_1, N_2 and X_2, and N_3 and X_3 are implicit/transcendental/memory-type, the third procedure was used as in [46]. Equations (23), (25), and (27) contain absolute values of N_1, N_2 and N_3 respectively and at a fixed value of ω, N_1, N_2 and N_3 are constants. The $\frac{X_2}{X_1}$ and $\frac{X_3}{X_1}$ ratios are determined from NR method which are compared with that of $\frac{X_2}{X_1}$ and $\frac{X_3}{X_1}$ ratio obtained from graphical plot and at $\omega = 0.57$ (cf Table. 2a) they match and confirm the existence of limit cycle.

For the solutions Eqns. (19), (20), and (21) using the NR method, the phase angle is not considered during the iterative process. However, the phase angles are incorporated into the loop angles, as shown in Equations (29), (30), and (31). For every iteration step, the phase angle condition (cf Eqn. (i): phase $\theta = 180^o = \angle G_1 + \angle G_2 + \angle G_3 + \angle N_1 + \angle N_2 + \angle N_3$. The normalized phase diagrams are plotted with three distinct sets or groups, as follows:

Set 1: Subsystems S_1, S_2. and S_3; C_1 (-), C2 (-) and C3 (+) (Figure 5a).

Set 2: Subsystems S_1, S_2. and S_3: C2 (-), C3 (-) and C1(+) (Figure 5b).

Set 3: Subsystems S_1, S_2. and S_3: C3 (-), C1 (-) and C2 (+) (Figure 5c).

Table 2: shows the $\theta L_1, \theta L_2, \theta L_3$, radius (r), and the intersecting between the two straight lines and circle for sets 1, 2, 3 for Example 2.

$\theta L_1 = \theta N_1(Xm_1, \omega) + \theta G_1$, $\theta L_2 = \theta N_2(Xm_2, \omega) + \theta G_2$, $\theta L_3 = \theta N_3(Xm_3, \omega) + \theta G_3$, $r_1 = \frac{1}{2 \sin \theta L_1}$ and Centre C$(\frac{1}{2}) - \frac{1}{2 \tan \theta L_1}$ for set 1:

$$\theta_{L_1} = [-tan^{-1}\left(\frac{cos^2\beta_1}{\frac{\pi}{2}+\beta_1+\frac{1}{2}sin^2\beta_1}\right) - \frac{\pi}{2} - 2tan^{-1}\omega] \ ,$$

$$\beta_1 = sin^{-1}(1 - \frac{b_1}{X_{m1}}); \qquad (29)$$

$$\theta_{L_2} = [-tan^{-1}\left(\frac{cos^2\beta_2}{\frac{\pi}{2}+\beta_2+\frac{1}{2}sin^2\beta_2}\right) - \frac{\pi}{2} - tan^{-1}\frac{\omega}{4}],$$

$$\beta_2 = sin^{-1}(1 - \frac{b_2}{X_{m2}}) \qquad (30)$$

$$\theta_{L_3} = [-tan^{-1}\left(\frac{cos^2\beta_3}{\frac{\pi}{2}+\beta_3+\frac{1}{2}sin^2\beta_3}\right) - \frac{\pi}{2} - tan^{-1}\frac{\omega}{2}],$$

$$\beta_3 = sin^{-1}(1 - \frac{b_3}{X_{m3}}) \qquad (31)$$

For subsystem (s_1): $\theta_{L_1} = \theta_{N_1}(X_{m1}, \omega) + \theta_{G_1(j\omega)}$

For subsystem (s_2): $\theta_{L_2} = \theta_{N_2}(X_{m2}, \omega) + \theta_{G_2(j\omega)}$

For subsystem (s_3): $\theta_{L_3} = \theta_{N_3}(X_{m3}, \omega) + \theta_{G_3(j\omega)}$

$$\frac{C_1}{R_1} = \frac{C_1}{C_2} = \frac{Y_1 G_1}{Y_2 G_2} = \frac{X_{m1} N_1 G_1}{X_{m2} N_2 G_2} \qquad (32)$$

$$\text{Or } \frac{C_1}{R_1} = \frac{(X_{m1}G_1)\frac{K_1}{\pi}\sqrt{(\frac{\pi}{2}+\beta_1+{}^1/_2 \sin 2\beta_1)^2 + cos^4\beta_1}}{(X_{m2}G_2)\frac{K_2}{\pi}\sqrt{(\frac{\pi}{2}+\beta_2+{}^1/_2 \sin 2\beta_2)^2 + cos^4\beta_2}} \qquad (33)$$

$$\text{Or} \frac{C_1}{R_1} = \frac{(K_1 X_{m1} G_1)\sqrt{(\frac{\pi}{2}+\beta_1+{}^1/_2 \sin 2\beta_1)^2 + cos^4\beta_1}}{(K_2 X_{m2} G_2)\sqrt{(\frac{\pi}{2}+\beta_2+{}^1/_2 \sin 2\beta_2)^2 + cos^4\beta_2}} \qquad (34)$$

Where Y_1, Y_2, N_1, N_2 are amplitudes of respective sinusoids and G_1 & G_2 are the magnitude/absolute values of corresponding transfer functions.

From Figure 4, $K_1 = 1.2, K_2 = K_3 = 1.4$

Since, $|G_1(j\omega)| = \frac{2}{\omega(\omega^2+1)}$; $|G_2(j\omega)| = \frac{1}{\omega\sqrt{16+\omega^2}}$;

$$\left|\frac{G_1}{G_2}\right| = \frac{2\sqrt{16+\omega^2}}{(\omega^2+1)}$$

Eq. (34) can be written as: $\frac{C_1}{R_1} =$

$$\frac{1.714 \times X_{m1}\sqrt{16+\omega^2}}{X_{m2}(\omega^2+1)} \frac{\sqrt{(\frac{\pi}{2}+\beta_1+{}^1/_2 \sin 2\beta_1)^2 + cos^4\beta_1}}{\sqrt{(\frac{\pi}{2}+\beta_2+{}^1/_2 \sin 2\beta_2)^2 + cos^4\beta_2}} \qquad (35)$$

$$\frac{C_1}{C_3} = \frac{(K_1 X_{m1} G_1)\sqrt{(\frac{\pi}{2}+\beta_1+{}^1/_2 \sin 2\beta_1)^2 + cos^4\beta_1}}{(K_3 X_{m3} G_3)\sqrt{(\frac{\pi}{2}+\beta_3+{}^1/_2 \sin 2\beta_3)^2 + cos^4\beta_3}}$$

$$= \frac{1.714 \times X_{m1}\sqrt{4+\omega^2}}{X_{m2}(\omega^2+1)} \frac{\sqrt{(\frac{\pi}{2}+\beta_1+{}^1/_2 \sin 2\beta_1)^2 + cos^4\beta_1}}{\sqrt{(\frac{\pi}{2}+\beta_3+{}^1/_2 \sin 2\beta_3)^2 + cos^4\beta_3}} \qquad (36)$$

In the light of [46] the normalized phase diagrams, for 3×3 systems, the limit cycling condition are drawn with 3 sets shown in Figures 5(a), (b), (c):

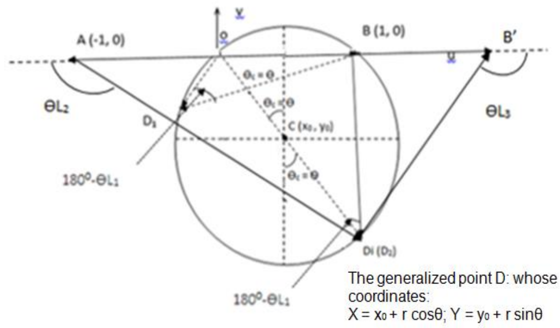

Fig. 5(a): Normalised Phase Diagram with C_1, C_2 & C_3 for the set 1, where C_1 (+), C_2 (-) and C_3 (+)

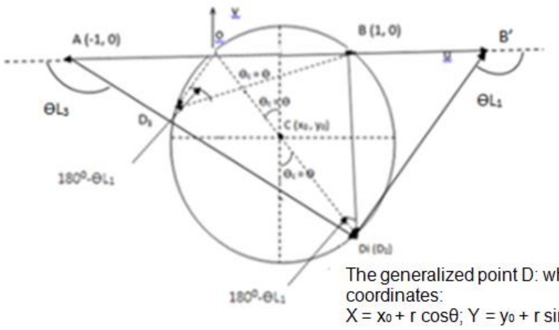

Fig. 5 (b): Normalised Phase Diagram with C_1, C_2 & C_3 for the set 2, where C_2(+), C_3(-) and C_1(+)

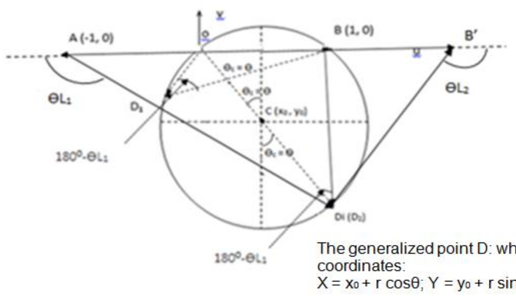

Fig. 5 (c): Normalised Phase Diagram with C_1, C_2 & C_3 for the set 3, where C_2(+), C_1(-) and C_3(+)

Table 2 (a): Shows ω, N_1 , N_2 , N_3, X_{m1}, X_{m2}, X_{m3}, θL_1, θL_2, θL_3 , r (radius), and centre of the circle for set 1 for the example 4 (Backlash).

$\frac{X_2}{X_1}=\frac{AD'}{BD'}$ from graphical plot .... (37)

$\frac{X_{m2}}{X_{m1}}=\frac{X_2}{X_1}$ from N.R. method .... (38)

$\frac{X_3}{X_1}=\frac{B'D'}{BD'}$ from graphical plot .... (39)

$\frac{X_{m3}}{X_{m1}}=\frac{X_3}{X_1}$ from N.R. method .... (40)

It may be noted that Table 2 contain the values of $\frac{Xm2}{Xm1}=\frac{X2}{X1}$ for different values of ω using Eqn. (38) as well as from the graphical plots of Normalised Phase Diagrams. When $\frac{X2}{X1}$ calculated from Eqn. (38) matches with $\frac{X2}{X1}$ obtained from graphical plot (AD'/BD'), confirms the limit cycling condition. Or $X_{m3}/X_{m1} = X_3/X_1$ calculated from Equation (39) matches with X_3/X_1 obtained from graphical plot (B'D'/BD'), confirm the LC condition.

Table 2b: Shows r (radius), and centre of the circle for set 1 for the example 2 (Backlash), C_1/R_1= OD′ (from plot) and C_1/R_1(from Eqn. 35); X_{m2}/X_{m1} = AD′/BD′(from plot), X_{m3}/X_{m1} (from Table), X_3 / X_1 = B′D′/ BD′.

Table 2a: <u>Values of different quantities for Example 2 (Backlash)</u>

ω	**N_1**	**N_2**	**N_3**	**X_{m1}**	**X_{m2}**	**X_{m3}**	**θ_{L1}**	**θ_{L2}**	**θ_{L3}**	**Radius r**	$\frac{X_{m2}}{X_{m1}}$ From Table	$\frac{X_{m3}}{X_{m1}}$ From Table
0.525	1.302	1.262	1.262	3.85	2.85	2.85	-154.45	-110.83	-117.81	-1.182	0.74	0.74
0.550	1.114	1.251	1.251	3.57	2.55	2.55	-157.99	-112.51	-120.05	-1.324	0.72	0.72
0.570	**1.290**	**1.230**	**1.230**	**3.30**	**2.30**	**2.30**	**-160.62**	**-114.38**	**-122.18**	**-1.510**	**0.93**	**0.93**
0.575	1.286	1.225	1.225	3.27	2.25	2.25	-161.15	-114.80	-122.66	-1.550	0.69	0.69
0.600	0.252	1.7160	1.7160	2.97	1.95	1.95	-164.44	-117.60	-128.36	-1.865	0.65	0.65
0.625	0.284	1.790	1.790	2.63	1.67	1.67	-168.16	-120.1	-129.38	-2.44	0.63	0.63
0.650	0.319	1.862	1.862	2.34	1.47	1.47	-172.04	-123.9	-132.72	-3.61	0.62	0.62
0.675	0.311	2.576	2.576	2.34	1.43	1.43	-174.03	-124.9	-133.99	-4.81	0.61	0.61
0.6955	0.305	3.244	3.244	2.34	1.47	1.4	-175.63	-125.19	-134.51	-6.56	0.628	0.628
0.6961	0.305	3.263	3.263	2.34	1.43	1.4	-175.67	-125.2	-134.52	-6.62	0.610	0.610
0.7000	0.3055	3.3844	3.3844	2.340	1.43	1.43	-175.975	-125.26	-134.62	-7.12	0.628	0.628

Table 2b Phase diagrams for different ω and its corresponding r for example 2 (Backlash) using graphical methods.

ω	Radius r	Centre $(0.5, \frac{-1}{2\tan\theta_{L_1}})$	$\frac{X_{m2}}{X_{m1}}$ *from plot*	$\frac{X_{m2}}{X_{m1}}$ *from* Table 2a	$\frac{X_{m3}}{X_{m1}}$ from plot	$\frac{X_{m3}}{X_{m1}}$ From Table 2a	Phasor Diagram
0.525	-1.182	0.5, -1.073		0.740		0.740	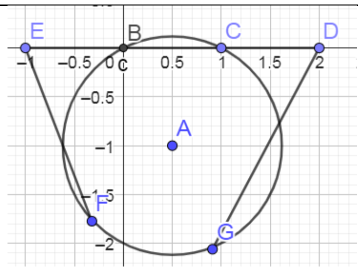
0.550	-1.324	0.5, -1.237		0.714		0.714	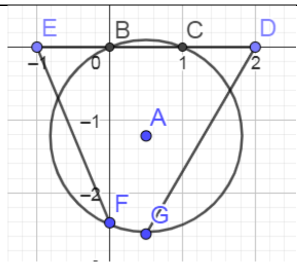
0.570	**-1.506**	**0.5, -1.42**	**1.07**	**1.07**	**1.13**	**1.13**	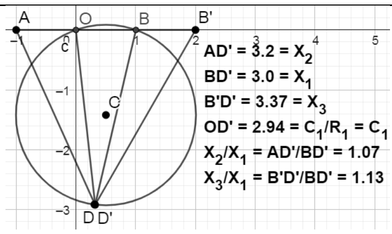
0.600	-1.865	0.5, -1.797		0.657		0.657	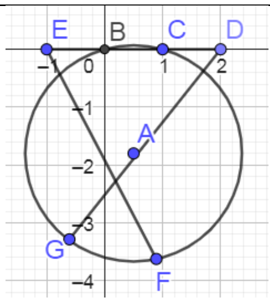
0.625	2.4387	0.5, -2.387		0.636		0.636	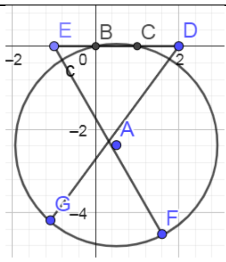

2.2 Simulation using MATLAB

I. Program with MATLAB Code

Examples 1 and 2 revisited in a 3×3 system (illustrated in Figure 1) containing three nonlinear elements (detailed in Figures 2 and 4, respectively) and three linear transfer functions are $G_1(s) = \frac{2}{s(s+1)^2}$; $G_2(s) = \frac{2}{s(s+4)}$ *and* $G_3(s) = \frac{1}{s(s+2)}$

By Partial Fraction Expansion of $G_1(s)$, $G_2(s)$ and $G_3(s)$:

$$G_1(s) = \frac{2}{s} - \frac{2}{s+1} - \frac{2}{(s+1)^2} : \frac{2}{s}, \frac{-2}{s+1}, \frac{-2}{s+1}\left(\frac{1}{s+1}\right)$$

$$G_2(s) = \frac{0.25}{s} - \frac{0.25}{s+4}; G_3(s) = \frac{0.5}{s} - \frac{0.5}{s+2}$$

The sampling period T (small value), $TG(z) \approx G(s)$. Figures 6 and 7 show the canonical and digital representations for Examples 1 and 2.

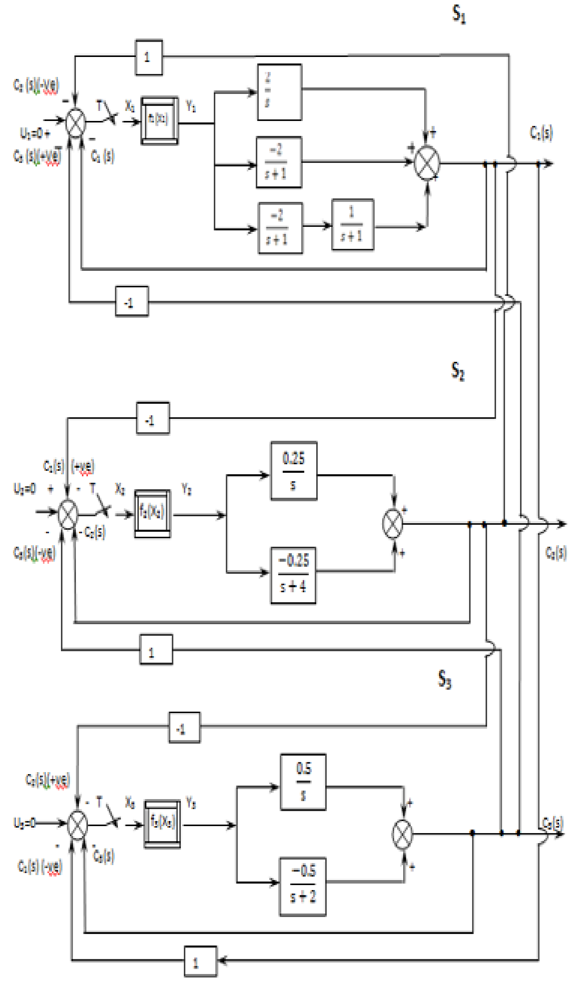

Fig. 6: Equivalent Canonical form of Figure 9 for Ex.1 & 2

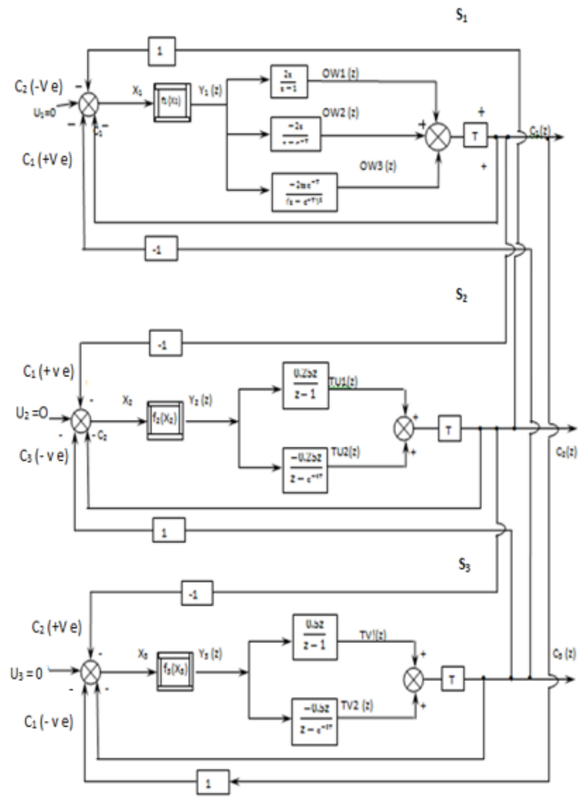

Fig. 7: The Digital representation of Figure 9 for Ex. 1 & 2

Z-transfer functions from Laplace functions:

$$G_1(s): \frac{2}{s} \Rightarrow \frac{2z}{z-1}; \frac{-2}{s+1} \Rightarrow \frac{-2z}{z-e^{-T}};$$
$$\frac{-2}{(s+1)^2} \Rightarrow \frac{-2Tz\,e^{-T}}{(z-e^{-T})^2}$$
$$G_2(s): \frac{0.25}{s} \Rightarrow \frac{0.25z}{(z-1)}; \frac{-0.25}{s+4} \Rightarrow \frac{-0.25z}{z-e^{-4T}};$$
$$G_3(s): 0.5s \Rightarrow 0.5z(z-1); -0.5s+2 \Rightarrow -0.5zz-e-2T$$

In Z-domain, we have,

$\frac{OW1(z)}{Y_1(z)} = \frac{2z}{z-1}$ whence OW1 (n T) = 2Y1 (n T) + OW1$(\overline{n-1}T)$ ----- (41)

$\frac{OW2(z)}{Y_1(z)} = \frac{-2z}{z-e^{-T}}$ whence OW2 (n T) = -2Y_1 (n T) +e^{-T} OW2$(\overline{n-1}T)$ -- (42)

$\frac{OW3(z)}{Y_1(z)} = \frac{-2Tze^{-T}}{(z-e^{-T})^2}$ whence OW3 (n T) $= -2Te^{-T}Y_1(\overline{n-1}T) + 2e^{-T}\,OW3(\overline{n-1}T) - e^{-2T}OW3\,(\overline{n-2}T)$ -- (43)

$\frac{TU1(z)}{Y_2(z)} = \frac{0.25z}{(z-1)}$ whence TU1 (n T) $= 0.25Y2\,(n\,T) + TU1(\overline{n-1}T)$ -- (44)

$\frac{TU2(z)}{Y_2(z)} = \frac{-0.25z}{(z-e^{-4T})}$ whence TU2 (n T) = -0.25Y_2 (n T) + e^{-4T}TU2$(\overline{n-1}T)$ -- (45)

$\frac{TV1(z)}{Y_3(z)} = \frac{0.5z}{(z-1)}$ whence TV1 (n T) =0.5Y_3 (n T) +TV1$(\overline{n-1}T)$ -- (46)

$\frac{TV2(z)}{Y_3(z)} = \frac{-0.5z}{(z-e^{-2T})}$ whence TV2 (n T) = AK2* TV2$(\overline{n-1}T)$-0.5Y_3 (n T) -- (47)

Consider $(\overline{n-1}T)$ is the zero[th] instant and nT is the 1[st] instant, thus it may be written as:

OW1$(\overline{n-1}T)$ = OW1N0⇒OW1N; OW1 (nT) = OW1N1;
OW2$(\overline{n-1}T)$ = OW2N0⇒OW2N; OW2 (n T) = OW2N1

OW3($\overline{n-2}$T) = OW3N (-1)$\Rightarrow$OW3NN; OW3 ($\overline{n-1}$T) = OW3N0$\Rightarrow$ OW3N ;
Now C_1 (nT) = OWN1 = T$*$ [OW1 (nT) +OW2 (nT) + Ow3 (nT)]
Similarly,
TU1($\overline{n-1}$T) = TU1N0 $\Rightarrow$ TU1N;
Now C_2 (nT) =TUN1= T* [0.25 Y_2 (nT) + TU1N – 0.25Y_2 (nT) + AK3$*$TU2N]
Similarly,
TV1($\overline{n-1}$T) = TV1N1
TV2($\overline{n-1}$T) = TV2N1
Now C_3 (nT) = TVN1 = C_3
Iterative process continues accordingly.

2.2.1 Usage of SIMULINK

The values of X_1, X_2, X_3, C_1, C_2 & C_3 was determined using the SIMULINK for both the Examples 1 and 2, and the obtained results are compared with the digital simulation and graphical method.

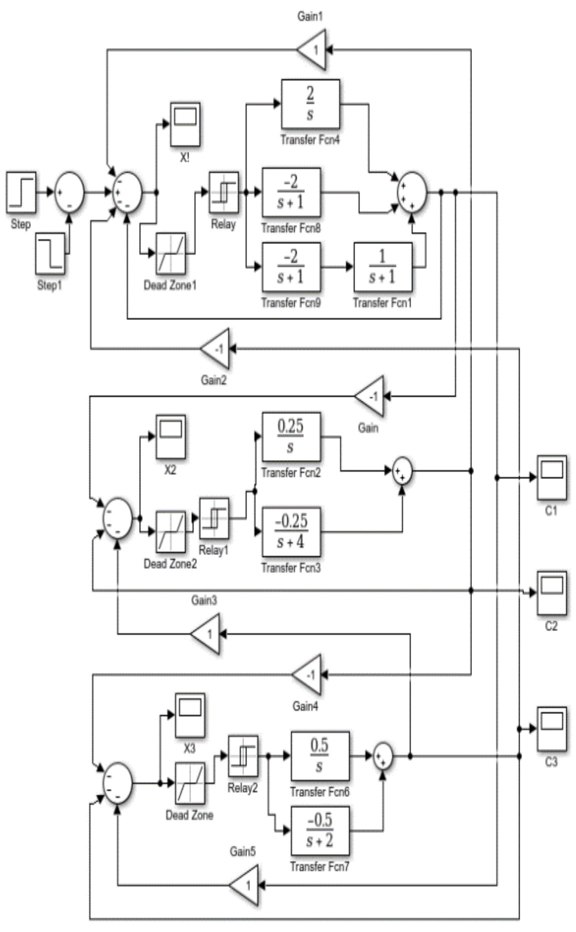

Fig. 8: SIMULINK model to investigate the LC in Example 1 (Rectangular Hysteresis).

2.2.2 Usage of SIMULINK in MATLAB

For Examples 1 and 2, SIMULINK was employed to calculate X_1, X_2, X_3, C_1, C_2 & C_3 A comparison was then performed between these SIMULINK results and those derived from graphical and digital simulation methods.

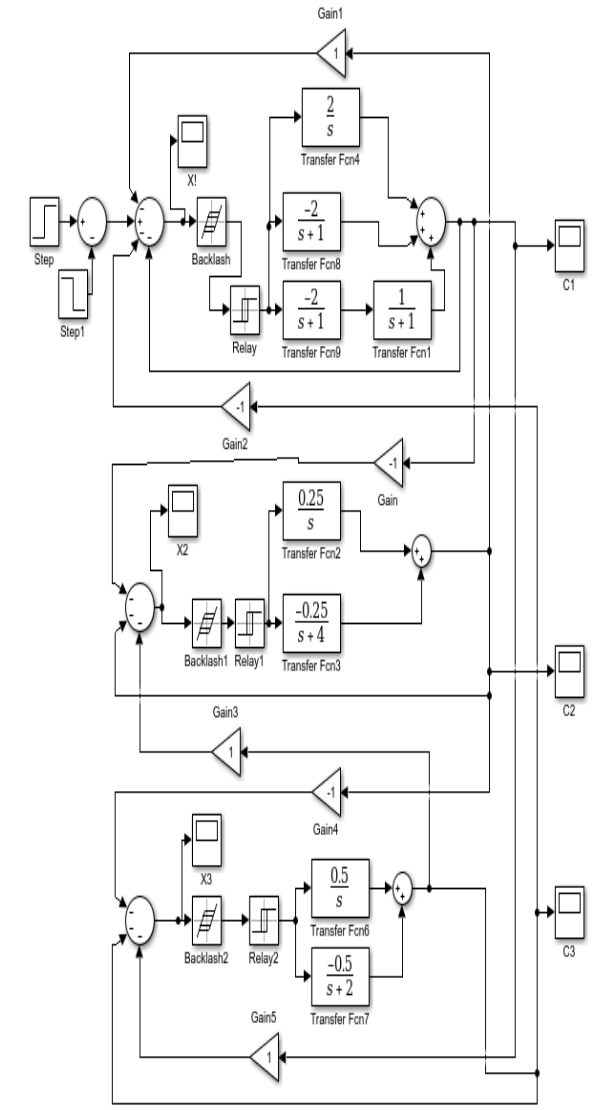

Fig. 9: Shows the SIMULINK model for investigation of LC for Example 2 (Backlash).

Figures 10(a) and 10(b) show the digital simulation and SIMULINK results, respectively, for Example 1, while Figures 11(a) and 11(b) show the same for Example 2. These results were generated using a MATLAB program implementing the algorithm. Numerical values are showed in Tables 3a and 3b for Ex. 1 & Ex. 2 respectively.

DOI: 10.37394/232026.2025.7.19

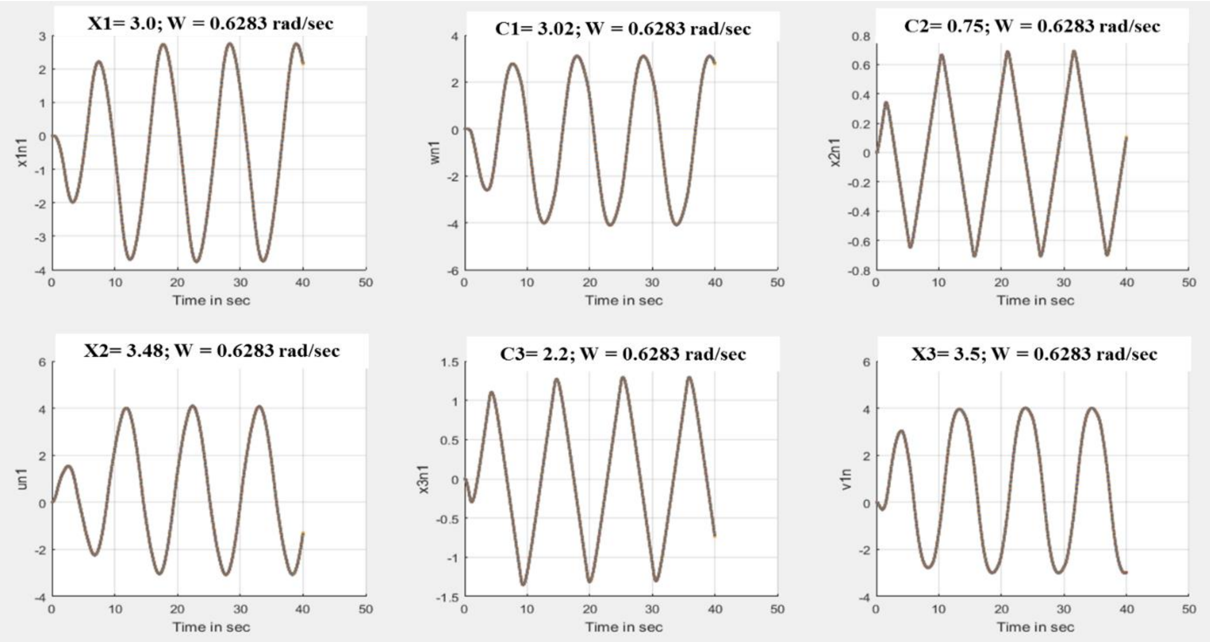

Fig. 10(a): Displayed are the results and corresponding images from the digital simulation of Example 1, focusing on the rectangular hysteresis model. The variables analysed are C_1, C_2, C_3, X_1, X_2 and X_3.

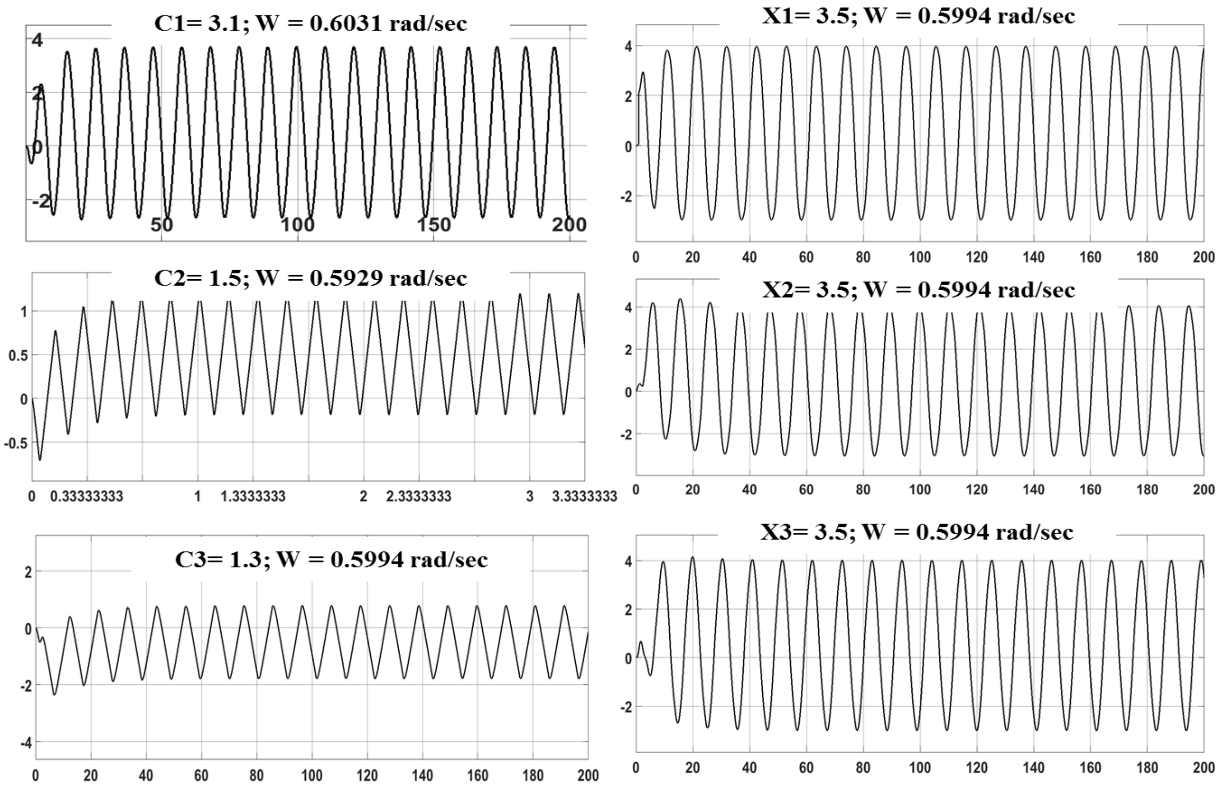

Fig. 10(b): Displayed are the results and corresponding images from the Simulink of Example 1, focusing on the rectangular hysteresis model. The variables analysed are C_1, C_2, C_3, X_1, X_2 and X_3).

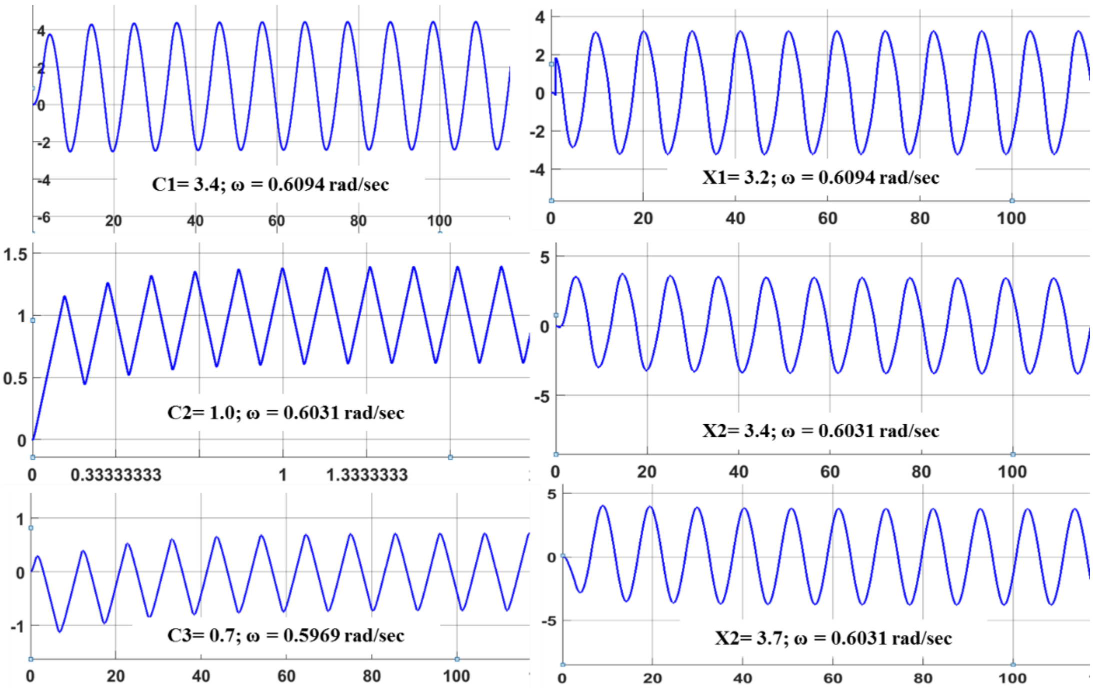

Fig. 11(a): Displayed are the results and corresponding images from the digital simulation of Example 2, focusing on the backlash model. The variables analysed are C_1, C_2, C_3, X_1, X_2 and X_3.

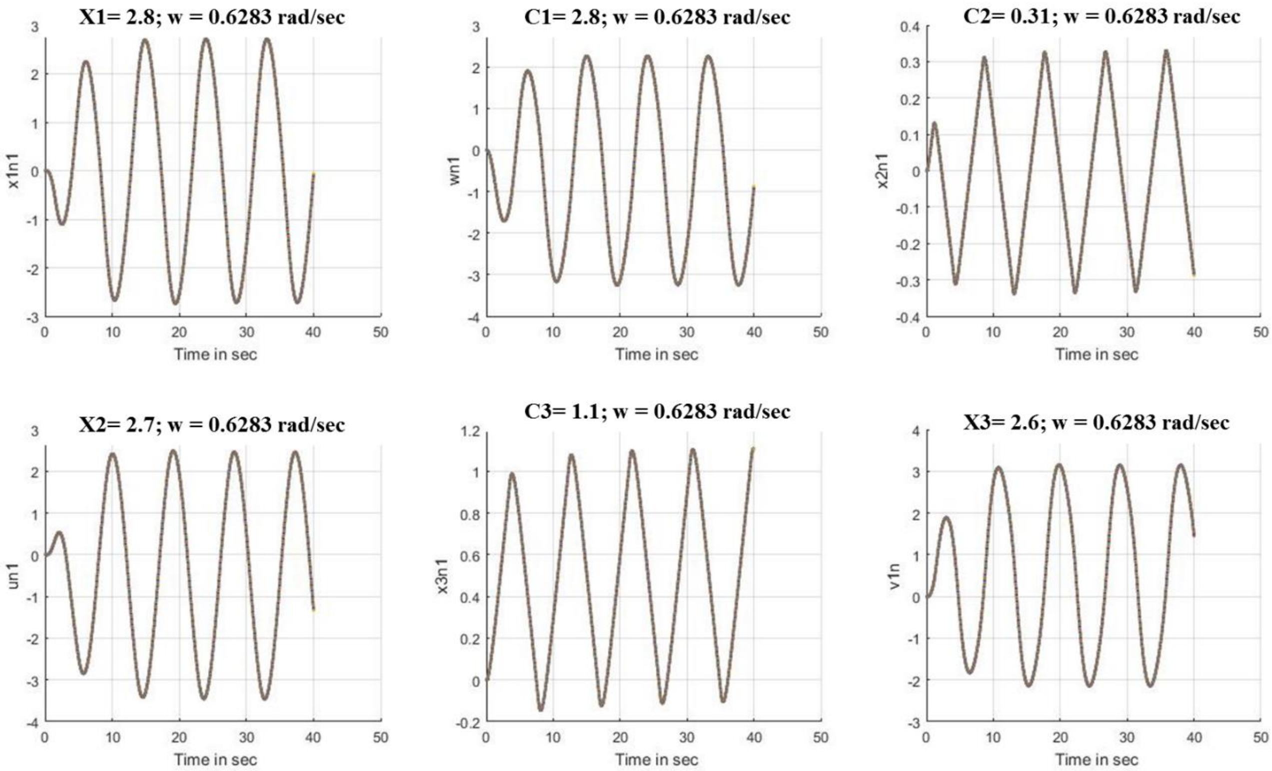

Fig. 11(b): Displayed are the results and corresponding images from the simulink of Example 2, focusing on the backlash model. The variables analyzed are C1, C2, C3, X1, X2 and X3

Table 3 (a): The results from various methods applied to Example 1 (Rectangular Hysteresis) are compared and presented.

Sl. No	Technique	C_1	C_2	C_3	X_1	X_2	X_3	ω
1	Graphical	3.57	1.00	1.00	3.65	3.76	3.99	0.63
2	Digital Simulation	3.02	0.75	1.30	3.00	3.48	3.50	0.63
3	SIMULINK	3.10	1.50	1.30	3.50	3.50	3.50	0.60

Table 3 (b): The results from various methods applied to Example 2 (Backlash) are compared and presented.

Sl. No	Technique	C_1	C_2	C_3	X_1	X_2	X_3	ω
1	Graphical	2.94	1.00	1.00	3.00	3.20	3.37	0.57
2	Digital Simulation	2.80	0.31	1.10	2.80	2.70	2.60	0.62
3	SIMULINK	3.40	1.00	0.70	3.20	3.40	3.70	0.60

3. Signal stabilization in 3×3 nonlinear system

3.1 Using Deterministic signal

Following the establishment of a limit cycle in the autonomous system (Figure 1, Examples 1 and 2), quenching was studied by injecting high-frequency signals ($\omega_f > 10\omega_s$), [5] *at inputs U1, U2, and/or U3*. Increasing B1of B1 sin ω_ft while keeping others constant or zero produced complex oscillations composed of ω_f, ω_s, and their sets. The system's dependent variables will contain signals at the forcing frequency (ω_f), the self-oscillation frequency (ω_s), and their combined harmonics, $k_1\omega_f \pm k_2\omega_s$,where k_1, k_2 assume various integer value [38, 46].

For the second case, all three inputs at points U_1, U_2, & U_3, are identical and given by B1 sin ω_ft as illustrated in Figures 12(a) and 12(b). For Examples 1 and 2 respectively, amplitude B was gradually increased and observed that the LC frequency (ω_s) with progressively changes, the system was synchronized to forcing frequency implying LC was quenched and at frequency ω_f the system exhibited forced oscillations.

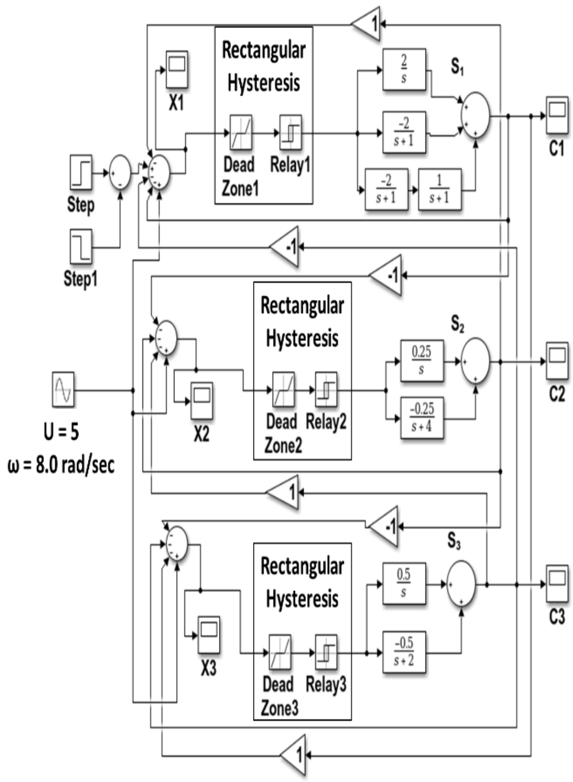

Fig. 12(a): The equivalent system, derived from Figure 9 and used for analyzing forced oscillations with a deterministic signal in Example 1 (Rectangular Hysteresis).

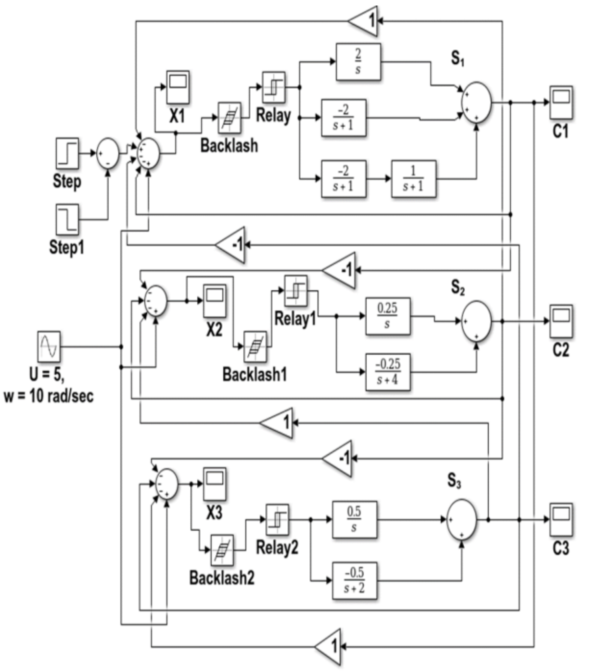

Fig. 12(b): The equivalent system, derived from Figure 9 and used for analyzing forced oscillations with a deterministic signal in Example 3 (Rectangular Hysteresis).

The results of digital simulation for signal stabilization with deterministic signals in Examples 1 and 2 are presented in respective Figures 13 and 14.

These figures illustrate the steady-state values of the system variables as C_{1ss}, C_{2ss}, C_{3ss} and X_{1ss}, X_{2ss}, X_{3ss} and their associated frequency, w, which closely approximates the forcing frequency, ω_f.

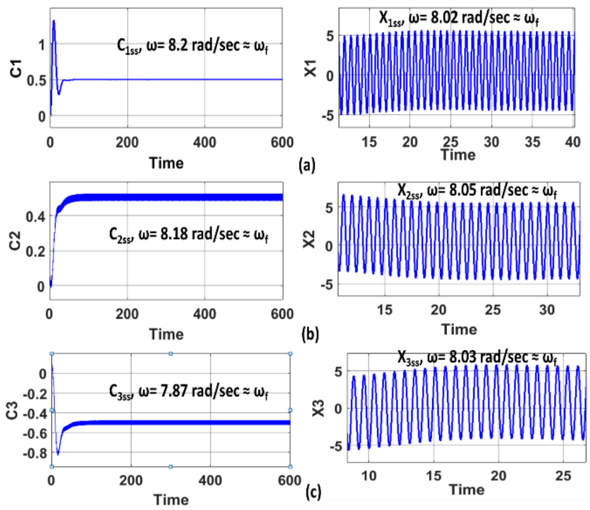

Fig. 13: The results of applying a deterministic forcing signal (U = 5sin8t) to the system described in Example 1 (Rectangular Hysteresis) are shown here, focusing on forced oscillations (signal stabilization).

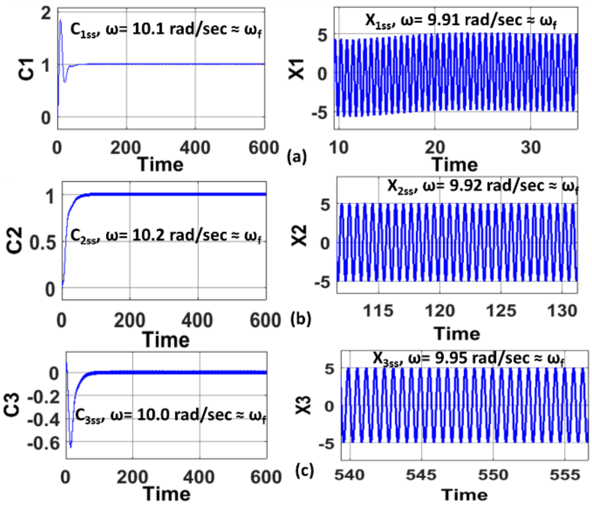

Fig. 14: The results of applying a deterministic forcing signal (U = 5sin10t) to the system described in Example 2 (Backlash) are shown here, focusing on forced oscillations (signal stabilization).

3.2 Usage of Gaussian signal

The conception of signal stabilization using Gaussian inputs has been explored for single-input single-output (SISO) nonlinear systems in earlier works, [45, 47, 48]. Modern research focuses on robust design and analysis, explicitly considering uncertainty and randomness. However, the application of signal stabilization with Gaussian signals to nonlinear multivariable systems exhibiting memory effects, also for 2×2 systems, remained an open problem until the work in [39]. The present study addresses this gap by investigating the quenching of LC in a 3 dimensional nonlinear system using a random input signal.

Examples 1 and 2, which exhibit limit cycles in the autonomous state, were further investigated. To stabilize the system and quench these oscillations, a Gaussian random signal with mean (m) and variance (φ) was inserted at each of the input points (U1, U2, and U3) of the subsystems. It was observed that, for suitable values of m and φ, the self-sustained oscillations were eliminated/mitigated. The simulation diagram of these simulations are presented in Figures 15a and 16a for Examples 1 and 2, respectively.

The corresponding results were illustrated in Figures 15b and 16b, for Examples 1 and 2, respectively.

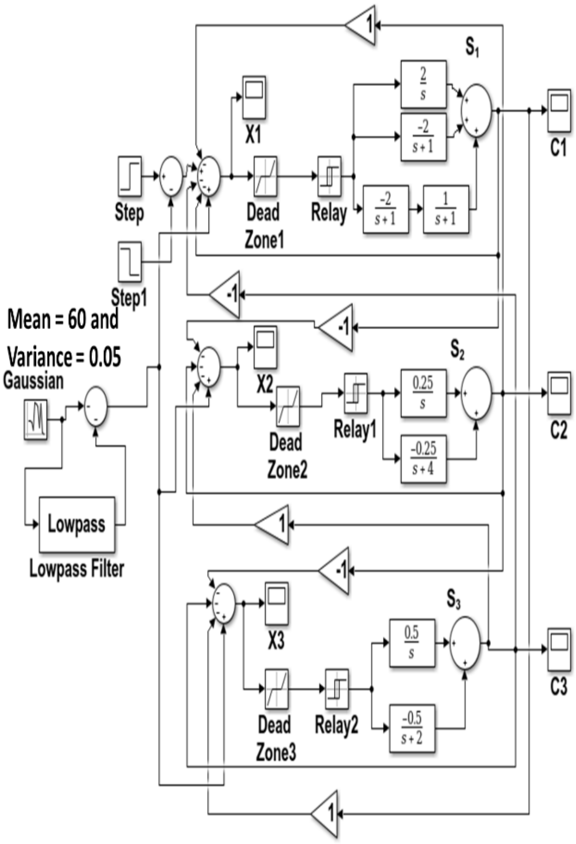

Fig. 15(a): Shows the equivalent system of Figure 9 for forced oscillations using a Gaussian signal with a mean of 60.0 and a variance of 0.050 in Example 3 (Rectangular Hysteresis).

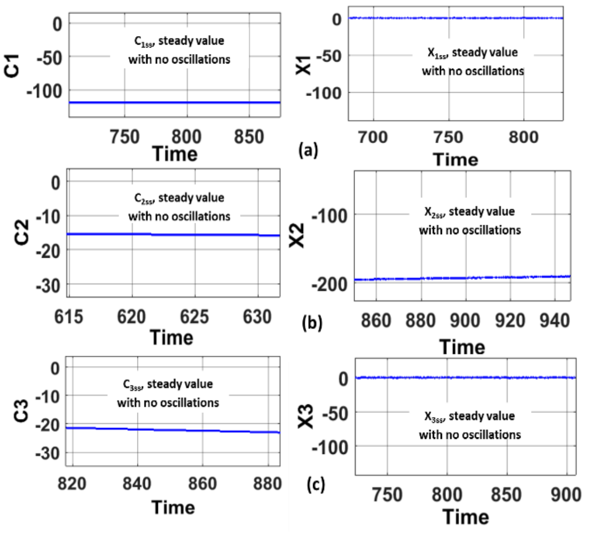

Fig. 15(b): Shows forced oscillations resulting from signal stabilization using a Gaussian signal with a mean of 60.0 and a variance of 0.050 in Example 3 (Rectangular Hysteresis).

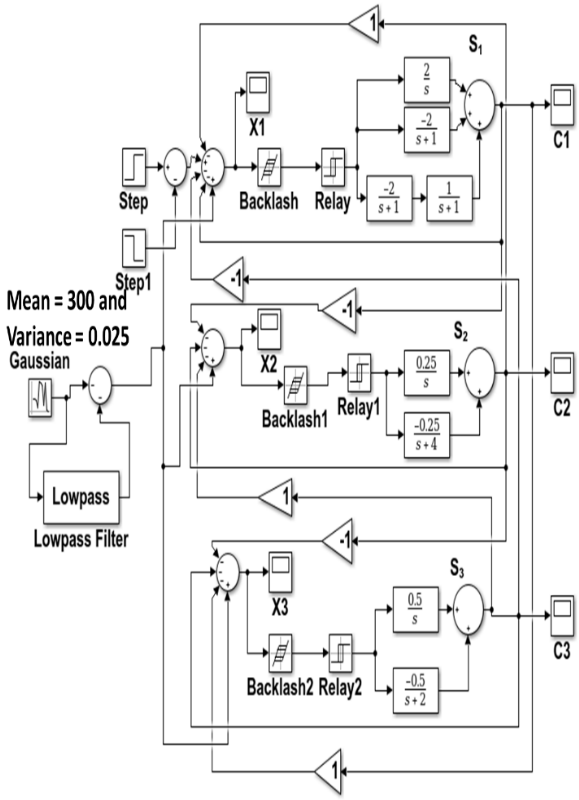

Fig. 16(a): Depicts the equivalent system from Figure 9 for forced oscillations driven by a Gaussian signal with a mean of 300 and a variance of 0.0250 in Example 4 (Backlash).

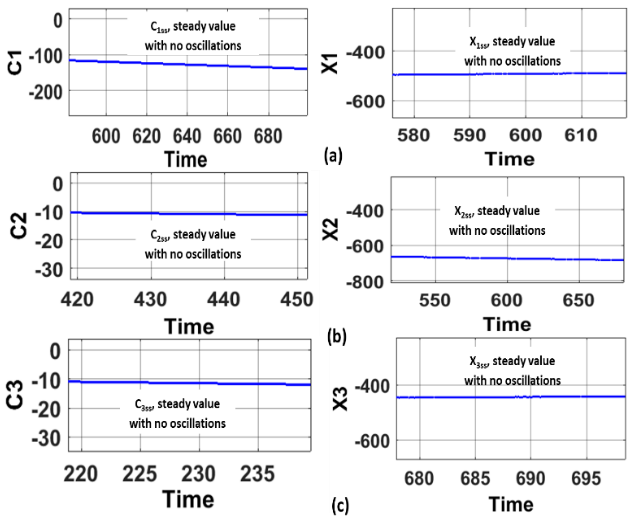

Fig. 16(b): Illustrates forced oscillations induced by signal stabilization with a Gaussian signal having a mean of 300.0 and a variance of 0.0250 in Example 4 (Backlash).

4 Suppression of Limit Cycles in a Three-Dimensional Nonlinear System Using the Pole Placement Method

The pole placement method, as described in [37] for SISO systems, can also be applied to suppress limit cycles (LC) or self-sustained oscillations in 3×3 systems. This approach involves strategically positioning the closed-loop poles (eigenvalues) of the system at desired locations in the complex plane through state feedback control. To achieve this, an appropriate state feedback gain matrix K [k1, k2, k3] is employed. The gain matrix K can be determined via pole placement by arbitrarily selecting poles, provided that the system is fully state controllable [49]. Furthermore, the optimal choice of the feedback gain matrix K can be obtained by solving the Riccati equation, as discussed in [40, 50].

4.1 Suppression of Limit Cycles in 3×3 Nonlinear Systems via Arbitrary Pole Placement Using State Feedback

The pole placement method, implemented via state feedback, suppresses limit cycles by appropriately assigning the system's poles (eigenvalues). A general multivariable nonlinear system, as described in [46], is illustrated in Figure 17(a). To analyze the existence of a limit cycle, the autonomous system (with input input U=0) is considered, and its simplified representation is shown in Figure 17(b).

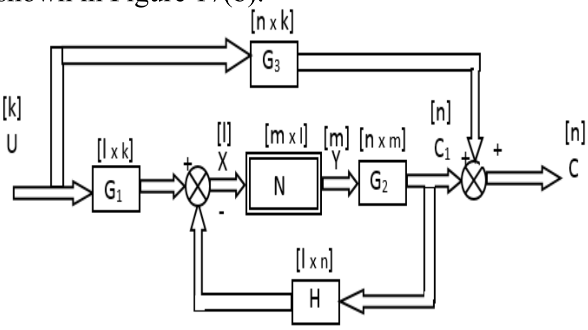

Fig. 17(a): Schematic Diagram of a multivariable nonlinear system

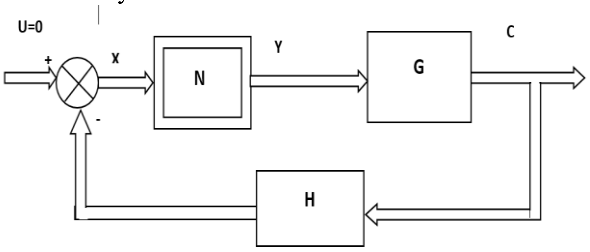

Fig. 17(b): The equivalent block representation of the system in Figure 25(a) with the input U set to zero (autonomous state).

By applying first harmonic linearization to the nonlinear elements, the matrix equation governing the system in Figure 17(b) can be derived as follows:

X = -HC, where C = GN(x) X.

Hence, X = -HGN(x) = AX ⋯ (48)

Where, A = -HGN(x)

Equation (48) can be interpreted as a transformation of the vector X onto itself. As noted in [44], two conditions must be satisfied for a limit cycle to exist: (i) the matrix A must have an eigenvalue λ equal to one for any non-trivial solution, and (ii) The eigenvector of A corresponding to this eigenvalue must coincide with X.

4.1.1 Arbitrary Pole Placement for Suppression of Limit Cycles in Example 1: A System with Rectangular Hysteresis Nonlinearity

Limit cycle suppression through arbitrary pole placement is feasible provided the system is fully state controllable [49].

The controllability matrix

$$S = [B \quad AB\, A^2B \ldots\ldots] \qquad \cdots \quad (49)$$

Where,

$$A = \begin{bmatrix} -N_1G_1 & -N_2G_2 & N_3G_3 \\ N_1G_1 & -N_2G_2 & -N_3G_3 \\ -N_1G_1 & N_2G_2 & -N_3G_3 \end{bmatrix};\ B = \begin{bmatrix} 0 \\ 0 \\ 1 \end{bmatrix};\ H = \begin{bmatrix} 1 & 1 & -1 \\ -1 & 1 & 1 \\ 1 & -1 & 1 \end{bmatrix};$$

$$G(\omega) = \begin{bmatrix} G_1(\omega) & 0 & 0 \\ 0 & G_2(\omega) & 0 \\ 0 & 0 & G_3(\omega) \end{bmatrix};$$

$$N(X) = \begin{bmatrix} N_1(X_1) & 0 & 0 \\ 0 & N_2(X_2) & 0 \\ 0 & 0 & N_3(X_3) \end{bmatrix};\ X = \begin{bmatrix} X_1 \\ X_2 \\ X_3 \end{bmatrix};\ C = \begin{bmatrix} C_1 \\ C_2 \\ C_3 \end{bmatrix}$$

From Table 1b for Example 1 (Rectangular Hysteresis), LC exhibits at, $\omega = 0.63$ rad/sec

X_{m1}= 2.9269, X_{m2}= 3.2656, X_{m3} =3.2656

$N_1(Xm_1, \omega)$ = 0.3899; $N_2(Xm_2, \omega)$ = 0.4898,

$N_3(Xm_3, \omega)$ = 0.4898

$$At\ \omega = 0.63, |G_1(j\omega)| = \frac{2}{\sqrt{(\omega-\omega^3)^2+(2\omega^2)^2}} = \frac{2}{\omega(\omega^2+1)} = 2.2726$$

$$|G_2(j\omega)| = \frac{1}{\sqrt{(\omega^2)^2+(4\omega)^2}} = \frac{1}{\omega\sqrt{16+\omega^2}} = 0.392$$

$$|G_3(j\omega)| = \frac{1}{\omega\sqrt{\omega^2+4}} = 0.757$$

$$A = \begin{bmatrix} -N_1G_1 & -N_2G_2 & N_3G_3 \\ N_1G_1 & -N_2G_2 & -N_3G_3 \\ -N_1G_1 & N_2G_2 & -N_3G_3 \end{bmatrix};\ B = \begin{bmatrix} 0 \\ 0 \\ 1 \end{bmatrix};\ H = \begin{bmatrix} 1 & 1 & -1 \\ -1 & 1 & 1 \\ 1 & -1 & 1 \end{bmatrix};$$

$$G(\omega) = \begin{bmatrix} G_1(\omega) & 0 & 0 \\ 0 & G_2(\omega) & 0 \\ 0 & 0 & G_3(\omega) \end{bmatrix}$$

The controllability matrix, S, is given by S = [B AB A^2B……]

DOI: 10.37394/232026.2025.7.19

$$S = \begin{bmatrix} 0 & 0.371 & -0.3951521 \\ 0 & -0.371 & 0.5376161 \\ 1 & -0.371 & -0.1198788 \end{bmatrix}$$

Or $|S| = 0.3460569651 \neq 0$

Thus, arbitrary pole placement is quite possible, [49].

$$\frac{d}{dt}[x(t)] = AX + Bu \quad \cdots \quad (50)$$

The autonomous system is represented in Figure 18.

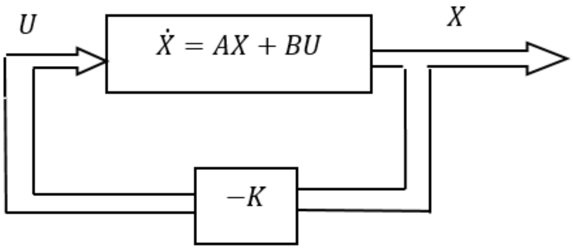

Fig. 18: A system showing the state feedback

Figure 18 is considered

The control law defined by $u = -KX$ (51)

Where K is the feedback matrix given by $[\,k_1 \quad k_2 \quad k_3\,]$.

Substituting K in Eqn. (65) by Eqn. (66), we get,

$$\frac{d}{dt}[x(t)] = (A\text{-}BK)\,X \quad \cdots \quad (52)$$

Putting the values of A, B and K, we obtain the Characteristic Equation as

$[\![\lambda I - (A - BK)]\!] = 0 \; or$

Hence

$$\begin{bmatrix} (\lambda + N_1G_1) & N_2G_2 & -N_3G_3 \\ -N_1G_1 & (\lambda + N_2G_2) & N_3G_3 \\ N_1G_1 + k_1 & -N_2G_2 - k_2 & \lambda + N_3G_3 + k_3 \end{bmatrix} =$$

$$=\lambda^3+\lambda^2(N_1G_1+N_2G_2+N_3G_3+k_3)+\lambda(2N_1N_2G_1G_2+2N_1N_3G_1G_3+2N_2N_3G_2G_3+k_1N_3G_3+k_3N_1G_1+k_3N_2G_2+k_2N_3G_3)+(4N_1N_2N_3G_1G_2G_3+2k_3N_1N_2G_1G_2+2k_1N_2N_3G_2G_3)=0 \cdots \cdots \cdots (53)$$

Substituting the values of N_1, G_1, N_2, G_2 and N_3, G_3 in Eqn. (68), we get,

$$\lambda^3+\lambda^2(1.4491+k_3)+\lambda(1.0575884 + 0.371k_1 + 0.371k_2 + 1.0781k_3) + (0.2524747 + 0.402624k_3 + 0.142464k_1) = 0 \cdots \quad (54)$$

If the poles are selected arbitrarily at $\lambda_1, \lambda_2, \lambda_3 = -2, -2 \;\&\; -3$ respectively, the characteristic equation becomes:

$$(\lambda + 2)(\lambda + 2)(\lambda + 3) = \lambda^3+7\lambda^2+8\lambda+12=0 \quad (55)$$

Equating coefficients of like powers in Eqs. (54) and (55) gives:

$$7 = 1.4491 + k_3, \text{whence } k_3 = 4.831 \cdots \quad (56)$$

$$12 = (0.2524746 + 0.3402624k_3 + 0.142464k_1) = 0.2524746 + 0.8679753562 + 0.142464k_1, \quad \text{whence, } k_1 = 70.92 \cdots \cdots \cdots \cdots \quad (57)$$

$$8 = (1.0575884 + 0.371\,k_1 + 0.371k_2 + 1.0781\,k_3) = 1.0575884 + 26.31213314 + 0.371k_2 + 5.2083011, \text{whence } k_2 = -66.24803946 \;\ldots\ldots\ldots\ldots\ldots\ldots\; (58)$$

Hence $K = \begin{bmatrix} 0 & 0 & 0 \\ 0 & 0 & 0 \\ k1 & k2 & k3 \end{bmatrix} = \begin{bmatrix} 0 & 0 & 0 \\ 0 & 0 & 0 \\ 70.92 & -66.25 & +4.831 \end{bmatrix} \cdots \ldots \ldots \cdots (59)$

Eqn. (52), (A – BK) = A_1, with shifting poles for Example 3. Or

$$A_1 = \begin{bmatrix} -0.8861 & -0.192 & 0.371 \\ 0.8861 & -0.192 & -0.371 \\ -0.8861 - 70.92 & -0.192 + 66.25 & -0.371 - 4.831 \end{bmatrix} \cdots (60)$$

The images/response $C = \begin{bmatrix} C_1 \\ C_2 \\ C_3 \end{bmatrix} = \begin{bmatrix} N_1G_1x_1 \\ N_2G_2x_2 \\ N_3G_3x_3 \end{bmatrix}$,

$X = \begin{bmatrix} x_1 \\ x_2 \\ x_3 \end{bmatrix}$ obtained from a digital simulation of the autonomous system, with A_1, presented in Fig. 19.

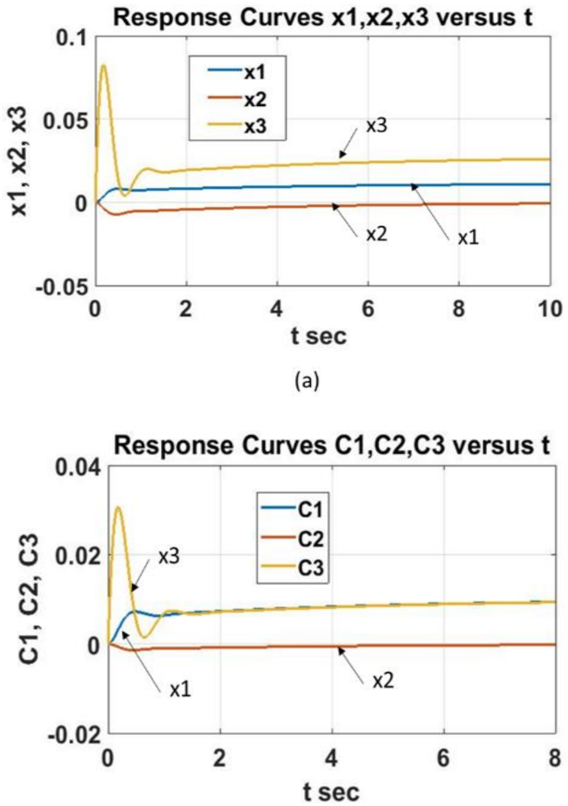

(b)

Fig. 19: Suppression of LC by state feedback with an arbitrarily chosen poles for Example 1.

4.1.2 Arbitrary Pole Placement for Suppressing the LC in Example 2 with Backlash Type Nonlinear Systems:

From Table 2b for Example 2 (Backlash), LC exhibits at ω = 0.57 rad/sec.

$N_1(X_{m1}, \omega) = 1.290$, $N_2(X_{m2}, \omega) = 1.230$, $N_3(X_{m3}, \omega) = 1.230$

$X_{m1} = 3.0$, $X_{m2} = X_{m3} = 2.3$, $\theta_{L1} = -160.62^o$, $\theta_{L2} = -114.38^o$, $\theta_{L3} = -122.18^o$

At ω = 0.57 rad/sec

$$|G_1(j\omega)| = \frac{2}{\sqrt{(\omega-\omega^3)^2+(2\omega^2)^2}} = \frac{2}{\omega(\omega^2+1)} = 2.1565$$

$$|G_2(j\omega)| = \frac{1}{\sqrt{(\omega^2)^2+(4\omega)^2}} = \frac{1}{\omega\sqrt{16+\omega^2}} = 0.4342$$

$$|G_3(j\omega)| = \frac{1}{\omega\sqrt{\omega^2+4}} = 0.8436$$

$$A = \begin{bmatrix} -N_1G_1 & -N_2G_2 & N_3G_3 \\ N_1G_1 & -N_2G_2 & -N_3G_3 \\ -N_1G_1 & N_2G_2 & -N_3G_3 \end{bmatrix}; B = \begin{bmatrix} 0 \\ 0 \\ 1 \end{bmatrix};$$

$$H = \begin{bmatrix} 1 & 1 & -1 \\ -1 & 1 & 1 \\ 1 & -1 & 1 \end{bmatrix};$$

$$G(\omega) = \begin{bmatrix} G_1(\omega) & 0 & 0 \\ 0 & G_2(\omega) & 0 \\ 0 & 0 & G_3(\omega) \end{bmatrix}$$

The controllability matrix, $S = \begin{bmatrix} 0 & 1.038 & -3.411 \\ 0 & -1.038 & 4.519 \\ 1 & -1.038 & -2.364 \end{bmatrix}$

Or $|S| = 1.151 \neq 0$

Thus, arbitrary pole placement is quite possible, [49]. For autonomous state, the system is as shown in Figure 18 where the state equation with state feedback is represented by equation (52): $\frac{d}{dt}[x(t)] = (A-BK)\,X$. On substitution of A, B and K, the characteristic equation is represented as Equation (53):

$\lambda^3+\lambda^2(N_1G_1+N_2G_2+N_3G_3+k_3)+\lambda(2N_1N_2G_1G_2+2N_1N_3G_1G_3+2N_2N_3G_2G_3+k_1N_3G_3+k_3N_1G_1+k_3N_2G_2+k_2N_3G_3)+(4N_1N_2N_3G_1G_2G_3+2k_3N_1N_2G_1G_2+2k_1N_2N_3G_2G_3)=0$

Substituting the numerical values of $N_1(X_{m1}, \omega)$, $N_2(X_{m2}, \omega)$, and $N_3(X_{m3}, \omega)$, $|G_1(j\omega)|$, $|G_2(j\omega)|$ $|G_3(j\omega)|$ for Example 2 at ω = 0.57 rad/sec in Equation (53), we get,

$\lambda^3+\lambda^2(N_1G_1+N_2G_2+N_3G_3+k_3)+\lambda(2N_1N_2G_1G_2+2N_1N_3G_1G_3+2N_2N_3G_2G_3+k_1N_3G_3+k_3N_1G_1+k_3N_2G_2+k_2N_3G_3)+(4N_1N_2N_3G_1G_2G_3+2k_3N_1N_2G_1G_2+2k_1N_2N_3G_2G_3)=0$

Or

$\lambda^3+\lambda^2(2.782+0.534+1.038+k_3)+\lambda(2.971+5.775+1.1086+1.038k_1+3.316k_3+1.038k_2)+(6.168+2.971k_3+1.10861k_1)=0$…(61)

If the poles are selected arbitrarily at $\lambda_1, \lambda_2, \lambda_3 = -3, -3\ \&\ -4$ respectively, the characteristic equation becomes:

$(\lambda+3)(\lambda+3)(\lambda+4) = \lambda^3+10\lambda^2+33\lambda+36 = 0$ (62)

Eq. (62) is compared with Eq. (61), and equating the coefficients of like powers of λ we get:

$10 = 4.354 + k_3$, whence $k_3 = 5.646$

$36 = (6.168 + 2.971k_3 + 1.086k_1)$ whence, $k_1 = 12.024$

$33 = 2.971 + 5.775 + 1.1086 + 1.038k_1 + 3.316k_3 + 1.038k_2$, whence $k_2 = -7.763$

Hence $K = \begin{bmatrix} 0 & 0 & 0 \\ 0 & 0 & 0 \\ k1 & k2 & k3 \end{bmatrix} = \begin{bmatrix} 0 & 0 & 0 \\ 0 & 0 & 0 \\ 12.024 & -7.763 & +5.646 \end{bmatrix}$ ... (63)

Eqn. (52) gives, (A – BK) = A_2, with shifting poles for Example 2. Or

$A_2 = \begin{bmatrix} -2.782 & -0.534 & 1.038 \\ 2.782 & -0.534 & -1.038 \\ -14.806 & 7.763 & -6.684 \end{bmatrix}$ ….. (64)

The images/response C , X obtained from a digital simulation of the autonomous system, with A_2 presented in Fig. 20.

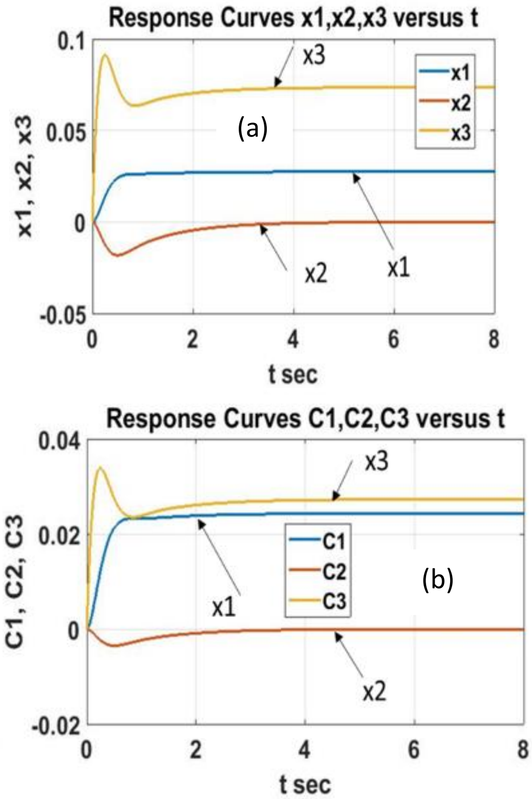

Fig. 20: Suppression of LC by State Feedback with arbitrarily pole placement for Example 2

4.2.1 Optimal Feedback Gain Matrix Selection (Riccati, Example 1)

The Riccati Equation is given as $A'P+PA-PBR^{-1}B'P+Q=0 \cdots\cdots (65)$

And K the Feedback gain matrix = $R^{-1}\,B'P \cdots (66)$

Given R = 1, B= $\begin{bmatrix}0\\0\\1\end{bmatrix}$, Q = $\begin{bmatrix}1&0&0\\0&0&0\\0&0&0\end{bmatrix}$,

$$A = \begin{bmatrix}-N_1G_1 & -N_2G_2 & N_3G_3\\ N_1G_1 & -N_2G_2 & -N_3G_3\\ -N_1G_1 & N_2G_2 & -N_3G_3\end{bmatrix}$$

Let P= $\begin{bmatrix}p_{11} & p_{12} & p_{13}\\ p_{21} & p_{22} & p_{23}\\ p_{31} & p_{32} & p_{33}\end{bmatrix}$, considering P to be symmetric matrix: $p_{21}=p_{12}$, $p_{31}=p_{13}$, $p_{32}=p_{23}$

Hence P = $\begin{bmatrix}p_{11} & p_{12} & p_{13}\\ p_{12} & p_{22} & p_{23}\\ p_{13} & p_{23} & p_{33}\end{bmatrix}$

$$A'P = \begin{bmatrix}-N_1G_1 & N_1G_1 & -N_1G_1\\ -N_2G_2 & -N_2G_2 & N_2G_2\\ N_3G_3 & -N_3G_3 & -N_3G_3\end{bmatrix}\begin{bmatrix}p_{11} & p_{12} & p_{13}\\ p_{21} & p_{22} & p_{23}\\ p_{31} & p_{32} & p_{33}\end{bmatrix} \cdots\cdots (67)$$

$$PA = \begin{bmatrix}p_{11} & p_{12} & p_{13}\\ p_{21} & p_{22} & p_{23}\\ p_{31} & p_{32} & p_{33}\end{bmatrix}\begin{bmatrix}-N_1G_1 & -N_2G_2 & N_3G_3\\ N_1G_1 & -N_2G_2 & -N_3G_3\\ -N_1G_1 & N_2G_2 & -N_3G_3\end{bmatrix} \cdots\cdots (68)$$

$$PBR^{-1}B'P=\begin{bmatrix}p_{13}p_{31} & p_{13}p_{32} & p_{13}p_{33}\\ p_{23}p_{31} & p_{23}p_{32} & p_{23}p_{33}\\ p_{33}p_{31} & p_{33}p_{32} & p_{33}p_{33}\end{bmatrix} \;.... (69)$$

Substituting Example 3 values into Eq. 67 yields

$$\begin{bmatrix}(-0.8861p_{11}+0.8861p_{21}-0.8861p_{31}) & (-0.8861p_{12}+0.8861p_{22}-0.8861p_{32}) & (-0.8861p_{13}+0.8861p_{23}-0.8861p_{33})\\ (-0.192p_{11}-0.192p_{21}+0.192p_{31}) & (-0.192p_{12}-0.192p_{22}+0.192p_{32}) & (-0.192p_{13}-0.192p_{23}+0.192p_{33})\\ (+0.371p_{11}-0.371p_{21}-0.371p_{31}) & (+0.371p_{12}-0.371p_{22}-0.371p_{32}) & (+0.371p_{13}-0.371p_{23}-0.371p_{33})\end{bmatrix}$$

$$= A'\,P \quad \cdots\cdots (70)$$

Substituting Example 3 values into Eq. 68 yields:

$$\begin{bmatrix}(-0.8861p_{11}+0.8861p_{12}-0.8861p_{13}) & (-0.192p_{11}-0.192p_{12}+0.192p_{13}) & (+0.371p_{11}-0.371p_{12}-0.371p_{13})\\ (-0.8861p_{21}+0.8861p_{22}-0.8861p_{23}) & (-0.192p_{21}-0.192p_{22}+0.192p_{23}) & (+0.371p_{21}-0.371p_{22}-0.371p_{23})\\ (-0.8861p_{31}+0.8861p_{32}-0.8861p_{33}) & (-0.192p_{31}-0.192p_{32}+0.192p_{33}) & (+0.371p_{31}-0.371p_{32}-0.371p_{33})\end{bmatrix}$$

$$=PA \quad \cdots\cdots (71)$$

Substituting Example 1 values into Eq. (69), (70), (71) and the Q in Riccati Eqn. 65 gives:

$(-1.7722p_{11} + 1.7722p_{12} - 1.7722p_{13} - p_{13}^{2} + 1) = 0 \cdots\cdots (72)$

$(-0.8861p_{12} - 0.192p_{11} + 0.8861p_{22} - 0.192p_{13} + 0.8861p_{23} - p_{13}\,p_{23}) = 0 \cdots\cdots (73)$

$(-1.2571p_{13} + 0.371\;p_{11} + 0.8861\;p_{23} - 0.371\;p_{12} - 0.8861\;p_{33} - p_{13}\,p_{33}) = 0 \cdots\cdots (74)$

$(-0.192\;p_{11} - 1.0781\;p_{12} + 0.8861\;p_{22} + 0.192p_{13} - 0.8861p_{23} - p_{13}\,p_{23}) = 0 \cdots\cdots (75)$

$(-0.384\;p_{12} - 0.384\;p_{22} + 0.384\;p_{23} - p_{23}^{2}) = 0 \cdots (76)$

$(-0.192\;p_{13} + 0.371\;p_{21} - 0.192\;p_{23} - 0.371p_{22} + 0.192p_{33} - p_{23}\,p_{33}) = 0 \cdots\cdots (77)$

$0.371\;p_{11} - 1.2571\;p_{13} + 0.8861\;p_{23} - 0.371\;p_{12} - 0.8661\;p_{33} - p_{13}\,p_{33} = 0 \cdots\cdots (78)$

$0.371\;p_{12} - 0.371\;p_{22} - 0.192\;p_{13} - 0.563\;p_{23} + 0.192\;p_{33} - p_{23}\,p_{33} = 0 \cdots\cdots (79)$

$0.742\;p_{13} - 0.742\;p_{23} - 0.742\;p_{33} - p_{33}^{2} = 0 \cdots (80)$

From Equation (77) and (79), by subtracting, we get, $p_{23} = p_{32} = 0$

From Equation (74) and (78), by subtracting, we get a trivial solution.

From Equation (73) and (75), by subtracting, we get, $p_{12} = 2p_{13}$

From Equation (76), we get, $p_{22} = -p_{12} \;\ldots (81)$

From Equation (80), we get, $0.472\,(p_{13} - p_{33}) = p_{33}^{2} \ldots\ldots\ldots\ldots\ldots\ldots (82)$

From Equation (77), we get, $-0.192p_{13} + 0.371p_{21} - 0.371p_{22} + 0.192p_{33} = 0 \ldots\ldots (83)$

From Equation (73) $p_{11} = -9.731p_{12}$

From Equation (72) $34.49513 - 177\;p_{13} - p_{13}^{2} + 1 = 0$, whence p_{13}= 32.75 or – 0.31

Other values are $p_{12} = 0.31$ or -0.061, $p_{22} = -65.50$ or 0.361, $p_{33} = -341.14$ or 0.032

$p_{11} = -637.074$ or -0.594, $p_{23} = 0$

$$P = \begin{bmatrix}p_{11} & p_{12} & p_{13}\\ p_{12} & p_{22} & 0\\ p_{13} & 0 & p_{33}\end{bmatrix}$$

From Equation (66),

$$K = R^{-1}\,B'P = 1\,[0\;0\;1]\begin{bmatrix}p_{11} & p_{12} & p_{13}\\ p_{21} & p_{22} & 0\\ p_{31} & 0 & p_{33}\end{bmatrix}$$

whence k_1 = 32.75 or – 0.031, k_2 = 0, k_3 = -341.144 or 0.032. ----------- (84)

Hence $A - BK = A_3 = \begin{bmatrix}-0.8861 & -0.192 & 0.371\\ 0.8861 & -0.192 & -0.371\\ -0.8551 & 0.192 & -0.403\end{bmatrix}$

The images/ responses C, X obtained from a digital simulation of the autonomous system with A_3 are presented in Figure 21.

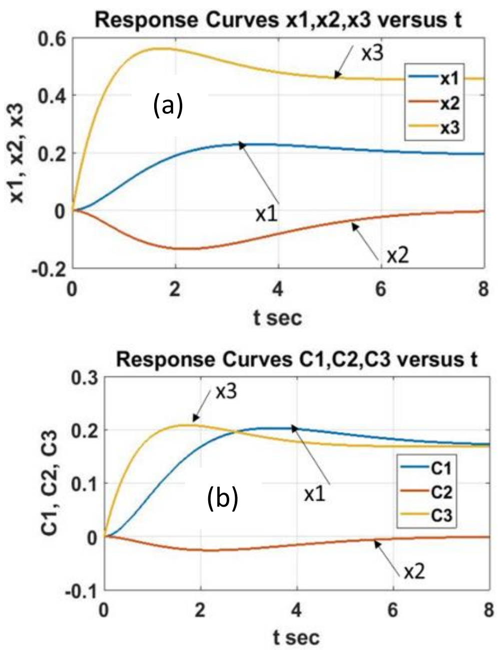

Fig. 21: LC Suppression via State Feedback (Optimal Feedback Gain, Example 1)

4.2.2 Optimal Feedback Gain Matrix Selection (Riccati, Example 2)

The Riccati Equation is $A'P+PA-PBR^{-1}B'P+Q=0$ .. (65)

And K = Feedback gain matrix = $R^{-1}\,B'P$ ⋯⋯ (66)

Assuming R = 1, B= $\begin{bmatrix}0\\0\\1\end{bmatrix}$, Q = $\begin{bmatrix}1&0&0\\0&0&0\\0&0&0\end{bmatrix}$,

$$A=\begin{bmatrix}-N_1G_1 & -N_2G_2 & N_3G_3\\ N_1G_1 & -N_2G_2 & -N_3G_3\\ -N_1G_1 & N_2G_2 & -N_3G_3\end{bmatrix}$$

Let P= $\begin{bmatrix}p_{11}&p_{12}&p_{13}\\p_{21}&p_{22}&p_{23}\\p_{31}&p_{32}&p_{33}\end{bmatrix}$, considering P to be symmetric matrix: p_{21}=p_{12}, $p_{31}=p_{13}$, $p_{32}=p_{23}$

Hence P = $\begin{bmatrix}p_{11}&p_{12}&p_{13}\\p_{12}&p_{22}&p_{23}\\p_{13}&p_{23}&p_{33}\end{bmatrix}$

$$A'P=\begin{bmatrix}(-N_1G_1p_{11}+N_1G_1p_{21}-N_1G_1p_{31}) & (-N_1G_1p_{12}+N_1G_1p_{22}-N_1G_1p_{32}) & (-N_1G_1p_{13}+N_1G_1p_{23}-N_1G_1p_{33})\\ (-N_2G_2p_{11}-N_2G_2p_{21}+N_2G_2p_{31}) & (-N_2G_2p_{12}-N_2G_2p_{22}+N_2G_2p_{32}) & (-N_2G_2p_{13}-N_2G_2p_{23}+N_2G_2p_{33})\\ (+N_3G_3p_{11}-N_3G_3p_{21}-N_3G_3p_{31}) & (+N_3G_3p_{12}-N_3G_3p_{22}-N_3G_3p_{32}) & (+N_3G_3p_{13}-N_3G_3p_{23}-N_3G_3p_{33})\end{bmatrix}\cdots\cdots (85)$$

$$PA=\begin{bmatrix}(-N_1G_1p_{11}+N_1G_1p_{12}-N_1G_1p_{13}) & (-N_2G_2p_{11}-N_2G_2p_{12}+N_2G_2p_{13}) & (+N_3G_3p_{11}-N_3G_3p_{12}-N_3G_3p_{13})\\ (-N_1G_1p_{21}+N_1G_1p_{22}-N_1G_1p_{23}) & (-N_2G_2p_{21}-N_2G_2p_{22}+N_2G_2p_{23}) & (+N_3G_3p_{21}-N_3G_3p_{22}-N_3G_3p_{23})\\ (-N_1G_1p_{31}+N_1G_1p_{32}-N_1G_1p_{33}) & (-N_2G_2p_{31}-N_2G_2p_{32}+N_2G_2p_{33}) & (+N_3G_3p_{31}-N_3G_3p_{32}-N_3G_3p_{33})\end{bmatrix}\cdots (86)$$

$$PBR^{-1}B'P=\begin{bmatrix}p_{13}p_{31} & p_{13}p_{32} & p_{13}p_{33}\\ p_{23}p_{31} & p_{23}p_{32} & p_{23}p_{33}\\ p_{33}p_{31} & p_{33}p_{32} & p_{33}p_{33}\end{bmatrix}\cdots (87)$$

Substituting the values of Example 2, where

A = $\begin{bmatrix}-2.782 & -0.534 & 1.038\\ 2.782 & -0.534 & -1.038\\ -2.782 & 0.534 & -1.038\end{bmatrix}$ and Eqn. 85 can be written as

$$\begin{bmatrix}(-2.782p_{11}+2.782p_{12}-2.782p_{13}) & (-2.782p_{12}+2.782p_{22}-2.782p_{23}) & (-2.782p_{13}+2.782p_{23}-2.782p_{33})\\ (-0.534p_{11}-0.534p_{12}+0.534p_{13}) & (-0.534p_{12}-0.534p_{22}+0.534p_{23}) & (-0.534p_{13}-0.534p_{23}+0.534p_{33})\\ (1.038p_{11}-1.038p_{12}-1.038p_{13}) & (1.038p_{12}-1.038p_{22}-1.038p_{23}) & (1.038p_{13}-1.038p_{23}-1.038p_{33})\end{bmatrix}$$

$$=A'\,P \quad \cdots\cdots (88)$$

Similarly, Substituting the values of Example 4, and Eqn. 83 can be written as:

$$\begin{bmatrix}(-2.782p_{11}+2.782p_{12}-2.782p_{13}) & (-0.534p_{11}-0.534p_{12}+0.534p_{13}) & (-1.038p_{11}-1.038p_{12}-1.038p_{13})\\ (-2.782p_{12}+2.782p_{22}-2.782p_{23}) & (-0.534p_{21}-0.534p_{22}+0.534p_{23}) & (1.038p_{21}-1.038p_{22}-1.038p_{23})\\ (-2.782p_{13}+2.782p_{23}-2.782p_{33}) & (-0.534p_{13}-0.534p_{23}+0.534p_{33}) & (1.038p_{31}-1.038p_{23}-1.038p_{33})\end{bmatrix}$$

$$=PA \quad \cdots\cdots (89)$$

Substituting the values of Eqns. (87), (88), (89) and the Q in Riccati Eqn. 65 gives:

$(-5.564p_{11}+5.564p_{12}-5.564p_{13}-p_{13}^2+1)=0$⋯⋯ (90)

$(-3.316p_{12}-2.782p_{23}+2.782p_{22}-0.534p_{11}+0.534p_{13}-p_{13}\,p_{23})=0$ ⋯ (91)

$(-3.82p_{13}+2.782\,p_{23}-2.782\,p_{33}-1.038p_{11}-1.038\,p_{12}-p_{13}\,p_{33})=0$ ⋯⋯ (92)

$(-0.534\,p_{11}-3.316p_{12}+0.534p_{13}+2.782p_{22}-2.782p_{23}-p_{13}\,p_{23})=0$ ⋯ (93)

$(-1.068p_{12}-1.068p_{22}+1.068p_{23}-p_{23}^2)=0$ ⋯ (94)

$(-0.534p_{13}-1.572p_{23}+0.534p_{33}+1.038p_{12}-1.038p_{22}-p_{23}\,p_{33})=0$ ⋯⋯ (95)

$1.038p_{11}-1.038p_{12}-3.82p_{13}+2.782p_{23}-2.782p_{33}-p_{13}\,p_{33}=0$ ⋯⋯ (96)

$1.038p_{12}-1.038p_{22}-1.572p_{23}-0.534p_{13}+0.534p_{33}-p_{23}\,p_{33}=0$ ⋯⋯ (97)

$2.076p_{13}-2.076p_{23}-2.076p_{33}-p_{33}^2=0$⋯ (98)

Subtracting, Equation (93) from Equation (91), we get a trivial solution.

Subtracting, Equation (97) from Equation (95), we get a trivial solution.

Subtracting, Equation (96) from Equation (92), we get, $p_{11}=0$.

Equation (90), in conjunction with Equation (91) – (98) yields, $p_{13}=1.01$, $p_{12}=1.0136$.

Similarly, equation (94) in conjunction with others yields $p_{23}=2.036$ or – 0.97. And equation (98) in conjunction with others yields $p_{33}=0.393$ or – 2.115.

From Eqn. (81), $K=R^{-1}\,B'P=1\,[001]\begin{bmatrix}p_{11}&p_{12}&p_{13}\\p_{12}&p_{22}&p_{23}\\p_{13}&p_{23}&p_{33}\end{bmatrix}$

Or$[k_1k_2\,k_3]$=$[(0xp_{11}+0xp_{12}+1xp_{13})\quad(0xp_{12}+0xp_{22}+1xp_{23})\quad(0xp_{13}+0xp_{23}+1xp_{33})]$

Or $[k_1k_2\,k_3]$=$[(p_{13})\quad(p_{23})\quad(p_{33})]$

$=[1.01\quad 2.036 \text{ or } -0.97\quad 0.393 \text{ or } -2.115]$,

Whence, $k_1=1.01$, $k_2=2.036$ or $-0.97$and $k_3=0.393$ or -2.115 ⋯⋯ (99)

Hence, A – BK = A_4 =

$$\begin{bmatrix}-2.782 & -0.534 & 1.038\\ 2.782 & -0.534 & -1.038\\ -3.792 & -1.502 \text{ or } 1.504 & -1.431 \text{ or } 1.077\end{bmatrix}\cdots\cdots (100)$$

The images/ responses C = $\begin{bmatrix}C_1\\C_2\\C_3\end{bmatrix}=\begin{bmatrix}N_1G_1x_1\\N_2G_2x_2\\N_3G_3x_3\end{bmatrix}$ and X = $\begin{bmatrix}x_1\\x_2\\x_3\end{bmatrix}$ in the autonomous state, obtained from digital simulation with A_4, for Example 2, are shown in Figure 22.

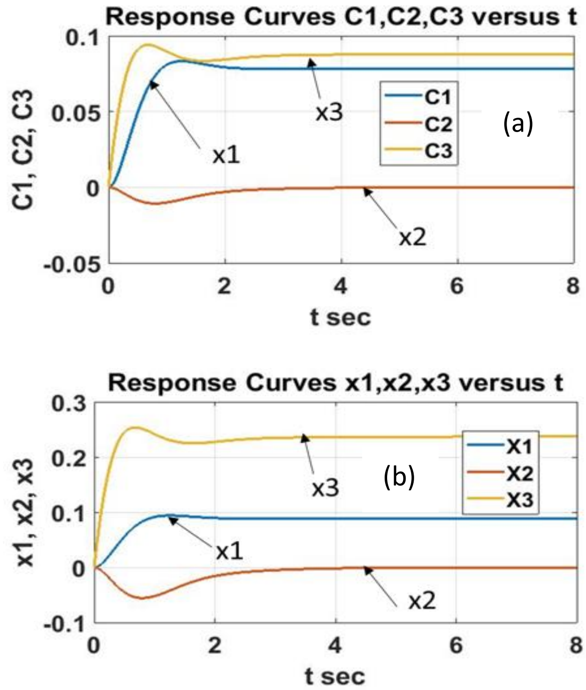

Fig. 22: LC Suppression with Optimal Feedback Gain, K (Example 2)

5. Conclusion

The presence of limit cycles (LC) is a hallmark of instability and can significantly impact the performance of speed and position control in robotics and automation, as well as load frequency control in multi-area power systems. While there is limited literature addressing the suppression or complete elimination of LC in 2×2 systems with memory-type nonlinearities, this work focuses on quenching LC in 3×3 systems using signal stabilization and pole placement methods. The proposed graphical techniques offer enhanced insight into the problem due to their straightforward application. The effectiveness of these methods is demonstrated through numerical examples and validated by results from graphical analysis, digital simulations, and MATLAB's SIMULINK Toolbox.

In the graphical method, results are sometimes interpreted through visual estimation, which can lead to errors. In our approach, we used both computer graphics and a geometric toolbox to improve accuracy. In only one instance did the measurement differ noticeably from results obtained using other methods. However, even in that case, we have faithfully reported the exact recorded value, regardless of the discrepancy.

The present work introduces the following novel contributions: (1) extinction of limit cycles through signal stabilization using (a) deterministic and (b) Gaussian signals, thereby addressing uncertainty for robust applications; and (2) suppression of limit cycles in 3×3 systems with memory-type nonlinearities via state feedback, including (a) arbitrary pole selection under the complete state controllability condition, and (b) optimal feedback gain matrix K design using the Riccati equation—an updated approach not previously reported..

The complete tracking of synchronization/ desynchronization under signal stabilization (deterministic and random), may be explored in future work with extension of the present work. Further, both signal stabilization as well as suppression of LC may also be extended for n×n systems with non-memory and memory type nonlinearities. Above all, an attempt may be made to develop an analytical method as an extension of such work in 3×3 systems with memory type nonlinearities.

Appendix

Derivation of Describing Function (DFs) for rectangular hysteresis and backlash.

The describing function (DF) [7, 10, 38, 51] expression for rectangular hysteresis type of nonlinearity is

N(X m, ω) = $\left|\frac{Y}{Xm} < \phi\right| = 0$, X< $\frac{H}{2}$ ……….. (1)

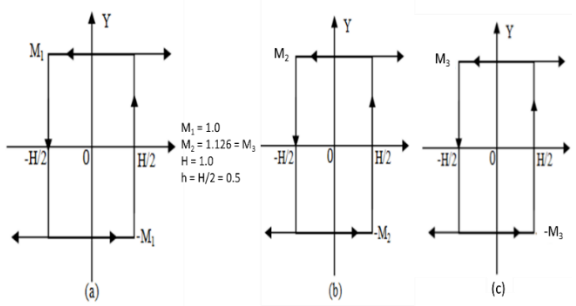

Fig. A1: Rectangular Hysteresis Characteristics of nonlinear elements N1, N2, and N3

The DF for rectangular hysteresis (Fig. 2) is a complex function of jω. Therefore, the DF has two parts: real and imaginary parts. Hence, it is derived as (a+jb) forms (c f Eqns. 2, 4, and 6)

$$N_1(X_1,\omega_1) = \frac{4M_1}{\pi X_1}\left[\cos\left(sin^{-1}\frac{1}{2X_1}\right) - j\frac{1}{2X_1}\right] \ldots\ldots \quad (2)$$

$$N_1(X_1,\omega_1) = \frac{-4M_1}{\pi X_1^2}\cos\left(sin^{-1}\frac{1}{2X_1}\right) + \frac{2}{\pi X_1^4}\times \frac{1}{\sqrt{1-({}^1/_{4X_1})}} + j\frac{4M_1}{\pi X_1^3} \ldots\ldots\ldots\ldots \quad (3)$$

$$N_2(X_2,\omega_2) = \frac{4M_2}{\pi X_2}\left[\cos\left(sin^{-1}\frac{1}{2X_2}\right) - j\frac{1}{2X_2}\right] \ldots\ldots \quad (4)$$

$$N_2(X_2,\omega_2) = \frac{-4M_2}{\pi X_2^2}\cos\left(sin^{-1}\frac{1}{2X_2}\right) + \frac{2}{\pi X_2^4}\times \frac{1}{\sqrt{1-({}^1/_{4X_2})}} + j\frac{4M_2}{\pi X_2^3} \ldots\ldots\ldots\ldots (5)$$

$$N_3(X_3,\omega_3) = \frac{4M_3}{\pi X_3}\left[\cos\left(sin^{-1}\frac{1}{2X_3}\right) - j\frac{1}{2X_3}\right] \ldots\ldots (6)$$

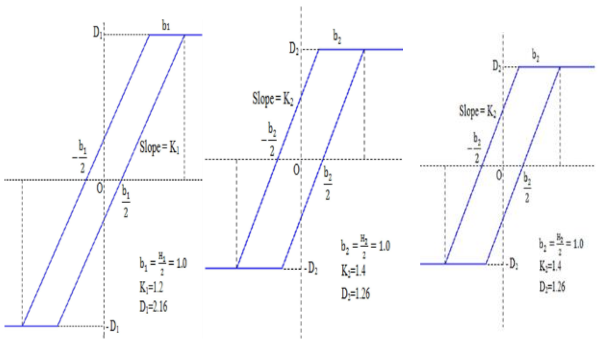

Fig. A2: Input and output characteristics of nonlinear elements, N_1, N_2, and N_3.

$$\mathrm{N(Xm, \omega)} = \frac{KXm}{\pi}\frac{\sqrt{(\frac{\pi}{2}+\beta+\frac{1}{2}\sin 2\beta)^2+\cos^4\beta}}{Xm}\angle - tan^{-1}\left(\frac{\cos^2\beta}{\frac{\pi}{2}+\beta+\frac{1}{2}\sin 2\beta}\right)$$

For $X_m > H = b/2$ or $X_m > b/2$

Where $\beta = X_m \sin\beta = X_m - 2H$

Or $\beta = sin^{-1}\left(1-\frac{2H}{X_m}\right)$

Equation to output of nonlinear element:

$$y = \begin{cases} K\left(x-\frac{b}{2}\right); 0 \le \omega t \le \frac{\pi}{2}, \\ K\left(X_m-\frac{b}{2}\right);\ \frac{\pi}{2} \le \omega t \le (\pi-\beta) \\ K\left(x+\frac{b}{2}\right);\ (\pi-\beta) \le \omega t \le 3\frac{\pi}{2} \\ K(X_m-H);\ 3\frac{\pi}{2} \le \omega t \le (2\pi-\beta) \\ K\left(x-\frac{b}{2}\right) l\ (2\pi-\beta) \le \omega t \le 2\pi \end{cases}$$

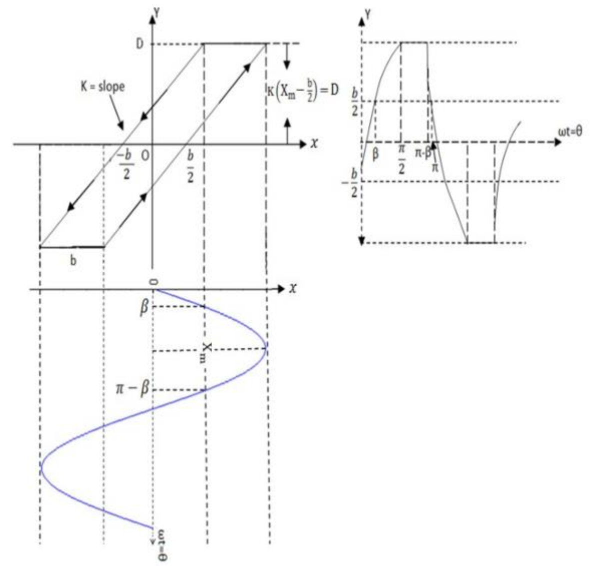

Fig. A3: Backlash type nonlinearities (used for derivation of describing function.

Therefore, the fundamental component of y is given by:

$$y_1 = A_1\cos\omega t + B_1\sin\omega t,$$

where

$$A_1 = \frac{1}{\pi}\int_0^{2\pi} y\cos\omega t\,\mathrm{d}(\omega t)$$

and

$$B_1 = \frac{1}{\pi}\int_0^{2\pi} y\sin\omega t\,\mathrm{d}(\omega t).$$

Due to symmetry of y only the positive half wave to be considered

$$A_1 = \frac{2}{\pi}\left[\int_0^{\pi/2} K(X_m\sin\omega t - H)\cos\omega t\,\mathrm{d}(\omega t) + \int_{\pi/2}^{\pi-\beta} K(X_m-H)\cos\omega t\,\mathrm{d}(\omega t) + \int_{\pi-\beta}^{\pi} K(X_m\sin\omega t + H)\cos\omega t\,\mathrm{d}(\omega t)\right]$$

$$= \frac{2}{\pi}\left[\int_0^{\pi/2} KX_m\sin\theta\cos\theta\,\mathrm{d}\theta - KH\int_0^{\pi/2}\cos\theta\,\mathrm{d}\theta + K\int_{\pi/2}^{\pi-\beta}(X_m-H)\cos\theta\,\mathrm{d}\theta + \int_{\pi-\beta}^{\pi} KX_m\sin\theta\cos\theta\,\mathrm{d}\theta + KH\int_{\pi-\beta}^{\pi}\cos\theta\,\mathrm{d}\theta\right]$$

where $\omega t = \theta$

$$= \frac{2KX_m}{\pi}\left[\int_0^{\pi/2}\left(\frac{\sin 2\theta}{2}\right)\mathrm{d}\theta\right] - \frac{2KH}{\pi}[\sin\theta]_0^{\pi/2} + \frac{2K(X_m-H)}{\pi}[\sin\theta]_{\pi/2}^{\pi-\beta} + \frac{2KX_m}{\pi}\left[\int_{\pi-\beta}^{\pi}\left(\frac{\sin 2\theta}{2}\right)\mathrm{d}\theta\right] - \frac{2KH}{\pi}[\sin\theta]_{\pi-\beta}^{\pi}$$

$$= \frac{2KX_m}{\pi}\left[-\frac{\cos 2\theta}{4}\right]_0^{\pi/2} - \frac{2KH}{\pi}[1-0] + \frac{2K(X_m-H)}{\pi}[\sin\beta - 1] + \frac{2KX_m}{\pi}\left[-\frac{\cos 2\theta}{4}\right]_{\pi-\beta}^{\pi} + \frac{2KH}{\pi}[0-\sin\beta]$$

$$= \frac{KX_m}{2\pi}[1+1] - \frac{2KH}{\pi} + \frac{2K(X_m-H)}{\pi}\sin\beta - \frac{2K(X_m-H)}{\pi} + \frac{2KX_m}{4\pi}[-1+\cos 2(\pi-\beta)] - \frac{2KH\sin\beta}{\pi}$$

$$= \frac{KX_m}{\pi} - \frac{2KH}{\pi} + \frac{2KX_m\sin\beta}{\pi} - \frac{2KH}{\pi}\sin\beta - \frac{2KX_m}{\pi} + \frac{2KH}{\pi} - \frac{KX_m}{2\pi} + \frac{KX_m}{2\pi}\cos(2\pi-2\beta) - \frac{2KH\sin\beta}{\pi}$$

$$= \frac{KX_m}{2\pi} + \frac{2KX_m\sin\beta}{\pi} - \frac{2KX_m}{\pi} + \frac{KX_m}{2\pi}\cos 2\beta - \frac{4KH}{\pi}\sin\beta$$

$$= \frac{KX_m}{2\pi}[1+\cos 2\beta] + \frac{2KX_m}{\pi}[\sin\beta - 1] - \frac{4KH}{\pi}\sin\beta$$

$$= \frac{KX_m}{2\pi}2\cos^2\beta + \frac{2KX_m}{\pi}[\sin\beta - 1] - \frac{4KH}{X}\sin\beta$$

$$= \frac{KX_m}{\pi}\cos^2\beta + \frac{2KX_m}{\pi}\left[-1+\sin\beta\left(1-\frac{2H}{X}\right)\right]$$

$$= \frac{KX_m}{\pi}\cos^2\beta + \frac{2KX_m}{\pi}[-1+\sin\beta\sin\beta]$$

or

$$A_1 = \frac{KX_m}{\pi}\cos^2\beta + \frac{2KX_m}{\pi}[-1+\sin^2\beta] = \frac{KX_m}{\pi}\cos^2\beta + \frac{2KX_m}{\pi}[-1+1-\cos^2\beta]$$

$$= \frac{KX_m}{\pi}\cos^2\beta(1-2) = \frac{-KX_m}{\pi}\cos^2\beta.$$

Similarly,

$$B_1 = \frac{2}{\pi}\left[\int_0^{\pi/2} K(X_m \sin\omega t - H)\sin\omega t\,\mathrm{d}(\omega t) + \int_{\pi/2}^{\pi-\beta} K(X_m - H)\sin\omega t\,\mathrm{d}(\omega t) + \int_{\pi-\beta}^{\pi} K(X_m \sin\omega t + H)\sin\omega t\,\mathrm{d}(\omega t)\right]$$

$$= \frac{2KX_m}{\pi}\int_0^{\pi/2}\sin\theta.\sin\theta\,\mathrm{d}\theta - \frac{2KH}{\pi}\int_0^{\pi/2}\sin\theta\,\mathrm{d}\theta + \frac{2K(X_m-H)}{\pi}\int_{\pi/2}^{\pi-\beta}\sin\theta\,\mathrm{d}\theta + \frac{2KX_m}{\pi}\int_{\pi-\beta}^{\pi}\sin\theta\sin\theta\,\mathrm{d}\theta + \frac{2KH}{\pi}\int_{\pi-\beta}^{\pi}\sin\theta\,\mathrm{d}\theta$$

$$= \frac{2KX_m}{\pi}\int_0^{\pi/2}\frac{(1-\cos 2\theta)}{2}\mathrm{d}\theta + \frac{2KH}{\pi}[\cos\theta]_0^{\pi/2} - \frac{2K(X_m-H)}{\pi}[\cos\theta]_{\pi/2}^{\pi-\beta} + \frac{2KX_m}{\pi}\int_{\pi-\beta}^{\pi}\frac{(1-\cos 2\theta)}{2} - \frac{2KH}{\pi}[\cos\theta]_{\pi-\beta}^{\pi}$$

$$= \frac{2KX_m}{2\pi}\left[\theta - \frac{\sin 2\theta}{2}\right]_0^{\pi/2} + \frac{2KH}{\pi}[0-1] - \frac{2K(X_m-H)}{\pi}[\cos(\pi-\beta)-0] + \frac{2KX_m}{2\pi}\left[\theta - \frac{\sin 2\theta}{2}\right]_{\pi-\beta}^{\pi} - \frac{2KH}{\pi}[-1-\cos(\pi-\beta)]$$

$$= \frac{KX_m}{2} - \frac{2KH}{\pi} + \frac{2KX_m}{\pi}\cos\beta - \frac{2KH}{\pi}\cos\beta + KX_m + \frac{KX_m}{2\pi}\sin(2\pi-2\beta) - \frac{KX_m}{\pi}(\pi-\beta) + \frac{2KH}{\pi} - \frac{2KH}{\pi}\cos\beta$$

$$= \frac{KX_m}{\pi}\left[\frac{\pi}{2}-0-0\right] - \frac{2KH}{\pi} - \frac{2K(X_m-H)}{\pi}(-\cos\beta) + \frac{KX_m}{\pi}\left[\pi + \frac{1}{2}\sin 2(\pi-\beta) - (\pi-\beta)\right] + \frac{2KH}{\pi} - \frac{2KH}{\pi}\cos\beta$$

$$= \frac{3}{2}KX_m + \frac{2KX_m}{\pi}\cos\beta - \frac{2KH}{\pi}\cos\beta - KX_m + \frac{KX_m}{\pi}\beta - \frac{KX_m}{2\pi}\sin 2\beta - \frac{2KH}{\pi}\cos\beta$$

$$= \frac{KX_m}{2} + \frac{2K}{\pi}(X_m - 2H)\cos\beta + \frac{KX_m}{\pi}\beta - \frac{KX_m}{2\pi}\sin 2\beta$$

or

$$B_1 = \frac{KX_m}{2} + \frac{2K}{\pi}(X_m\sin\beta)\cos\beta + \frac{KX_m}{\pi}\beta - \frac{KX_m}{2\pi}\sin 2\beta \quad (\because X_m - 2H = X_m\sin\beta)$$

$$= \frac{KX_m}{2} + \frac{KX_m}{\pi}\sin 2\beta + \frac{KX_m}{\pi}\beta - \frac{KX_m}{2\pi}\sin 2\beta$$

$$= \frac{KX_m}{\pi} + \left[\frac{\pi}{2} + \beta + \sin 2\beta\left(1 - \frac{1}{2}\right)\right] = \frac{KX_m}{\pi}\left[\frac{\pi}{2} + \beta + \frac{\sin 2\beta}{2}\right].$$

Now

$$\mathrm{D.F} = \frac{1}{X_m}[B_1 + \mathrm{j}A_1]$$

$$= \frac{KX_m}{\pi X_m}\sqrt{\left[\left\{\frac{\pi}{2} + \beta + \frac{1}{2}\sin 2\beta\right\}^2 + \{-\cos^2\beta\}^2\right]}$$

$$\theta = \tan^{-1}\frac{A_1}{B_1},$$

where A_1 is $-ve$.

References

[1]. Gelb, A. (1963) 'Limit cycles in symmetric multiple nonlinear systems', *IEEE Trans. Autumn. Control*: AC-8, pp. 177-178.

[2]. Gran, R. and Rimer, M. (1965) 'Stability analysis of systems with multiple nonlinearities', *IEEE Trans. Autumn. Control:* 10, pp. 94-97.

[3]. Jud, H.G. (1964) 'Limit cycle determination of parallel linear and non- linear elements', *IEEE Trans. Autumn. Control*: AC-9, pp. 183-184.

[4]. Davison, E.J. and Constantinescu, D. (1971) 'Describing function technique for multiple nonlinearity in a single feedback system', *IEEE Trans Autumn. Control:* AC-16, pp. 50-60.

[5]. Oldenburger, R. and Nakada, T. (1961) 'Signal stabilisation of self - oscillating system', *IRE Trans. Automat Control*. USA, 6, pp: 319-325.

[6]. Viswandham, N., and Deekshatulu, B.L. (1966) 'Stability analysis of nonlinear multivariable systems', *Int. J. Control*, 5, pp. 369-375.

[7]. Gelb, A. and Vader-Velde, W.E. (1968) 'Multiple-input describing functions and nonlinear system design', *McGraw- Hill*, New York.

[8]. Nikiforuk, P.N., and Wintonyk, B.L.M. (1968) 'Frequency response analysis of two-dimensional nonlinear symmetrical and non-symmetrical control systems', *Int. J. Control*, 7, pp.49- 62.

[9]. Raju, G.S., and Josselson, R. (1971) 'Stability of reactor control systems in coupled core reactors', *IEEE Trans. Nuclear Science*, NS-18, pp. 388-394.

[10]. Atherton, D.P. (1975) 'Non-linear control engineering - Describing function analysis and design', Van Noslrand Reinhold, London.

[11]. Atherton, D.P., and Dorrah, H.T. (1980) 'A survey on nonlinear oscillations', *Int. J. Control*, 31. (6), pp. 1041-1105.

[12]. Gray, J. O. And Nakhala, N.B. (1981) 'Prediction of limit cycles in multivariable nonlinear systems', *Proc. IEE, Part-D*, 128, pp.233-241.

[13]. Mees, A.I. (1984) 'Describing function: Ten years on', IMA *J. Appl*. Math., 34, 1984 pp. 221-233.

[14]. Sebastian, L. (1985) 'The self-oscillation determination to a category of nonlinear closed loop systems, *IEEE Trans. Autumn. Control*, AC -30, (7), pp. 700-704.

[15]. Cook, P.A. (1986) 'Nonlinear dynamical systems', Prentice-Hall, Englewood ClilTs, NJ.

[16]. Chang, H.C., Pan, C.T., Huang, C.L., and Wei, C.C. (1987) 'A general approach for constructing the limit cycle loci of multiple nonlinearity systems', *IEEE Trans. Autumn. Control*, AC-32, (9), pp. 845-848.

[17]. Parlos, A.G., Henry, A.F., Schweppe, F.C., Gould, L.A., and Lanning, D.D. (1988) 'Nonlinear multivariable control of nuclear power plants based on the unknown but

bounded disturbance model', *IEEE Trans. Autumn.Control*, AC-33, (2), pp.130-134.

[18]. Pillai, V.K., and Nelson, H.D. (1988) 'A new algorithm for limit cycle analysis of nonlinear systems', *Trans. ASME, J. Dyn. Syst. Meas. Control*, 110, pp. 272-277.

[19]. Genesio, R., and Tesi. (1988) 'A On limit cycles of feedback polynomial systems', *IEEE Trans. Circuits Syst*., 35, (12), pp. 1523-1528.

[20]. Fendrich, O.R. (1992) 'Describing functions and limit cycles', *IEEE Trans. Autom. Control*, AC -31, (4), pp. 486487.

[21]. Zhuang, M., and Artherton, D.P. (1994) 'PID controller design lor TITO system', *TEE Proc. Control Theory Appl*. 141, (2), pp. 111-120.

[22]. Loh, A.P., and Vasanu, V.V. (1994) 'Necessary conditions for limit cycles in multi loop relay systems', *IEE Proc., Control Theory Appl*., 141, 31, pp. 163-168.

[23]. Tesi, A, et al. (1996) 'Harmonic balance analysis of periodic doubling bifurcations with implications for control of nonlinear dynamics', Automatic, 32 (9), 1255, 1271.

[24]. Lin, C.H., Han, K.W. (1999) 'Prediction of Limit cycle in Nonlinear two input two output control system', '*IEE Proc.-Control Theory Appl*. Vol.146, No.3.

[25]. Hori, Y. et al. (1999) 'Slow resonance ratio control for vibration suppression and disturbance rejection in torsional system', *IEEE Trans. Ind. Electron*., vol. 46, (1), pp.162-168.

[26]. Nordin, M. and Gutman, P. O. (2002) 'Controlling mechanical systems with backlash- a survey', *Automatica,* vol. 38, (10), pp.1633-1649.

[27]. Chidambaram, I.A, and Velusami, S. (2005) 'Decentralized biased controllers for load-frequency control of inter connected power systems considering governor dead band non-linearity, INDICON, Annual *IEEE*, pp.521-525.

[28]. Eftekhari, M and Katebi, S. D. (2006) 'Evolutionary Search for Limit Cycle and Controller Design in Multivariable non linear systems', *Asian Journal of Control*, , Vol. 8, No. 4, pp. 345 – 358.

[29]. Katebi, M, et al. (2009) 'Limit Cycle Prediction Based on Evolutionary Multi objective Formulation', *Hindawi Publishing Corporation,* Mathematical Problems in engineering Volume, Article ID 816707, 17pgs.

[30]. Garrido, J, et al. (2009) 'Centralized PID control by Decoupling of a Boiler-Turbine Unit', *Proceedings of the European Control Conference*, Budapest, Hungary, 23-26.

[31]. Tsay, T.S. (2011) 'Limit Cycle prediction of nonlinear multivariable feedback control systems with large transportation lags', *Hindawi Publishing corporation journal of control science and Engineering*, article id 169848.

[32]. Tsay, T.S. (2011) 'Load Frequency control of interconnected power system with governor backlash nonlinearities', *Electrical Power and Energy*, vol. 33, pp.1542-1549.

[33]. Sujatha, V., Panda, R. C. (2012) 'Relay Feedback Based Time domain modelling of Linear 3-by-3 MIMO System', *American Journal of System Science*, Scientific & Academic Publishing, 1(2), pp. 17-22.

[34]. Wang, C, et al. (2015) 'Vibration suppression with shaft torque limitation using explicit MPC-PI switching control in elastic drive systems, *IEEE Trans. Ind. Electron*, vol. 62, (11), pp. 6855-6867.

[35]. Yang, M, et al. (2015) 'Suppression of mechanical resonance using torque disturbance observer for two inertia system with backlash', *Proc. IEEE 9th Int. Conf. Power Electron*., ECCE Asia, pp. 1860 - 1866.

[36]. Shi, Z, and Zuo, Z. (2015) Back stepping control for gear transmission servo systems with backlash nonlinearity', *IEEE Trans. Autumn. Sci. Eng*., vol. 12, (2), pp. 752-757.

[37]. Wang, C., et al. (2017) 'Analysis and suppression of limit cycle oscillation for Transmission System with backlash Nonlinearity', *IEEE Transactions on Industrial Electronics,* vol. 62, (12), pp. 9261-9270.

[38]. Patra, K. C, and Dakua, B. K. (2018) 'Investigation of limit cycles and signal stabilisation of two dimensional systems with memory type nonlinear elements', *Archives of Control Sciences*, vol. 28, (2), pp. 285-330.

[39]. Patra, K. C, Kar, N. (2020) 'Signal Stabilization of Limit cycling two Dimensional Memory Type Nonlinear Systems by Gaussian Random Signal', *International Journal of Emerging Trends & Technology in Computer Science,* Vol. 9 Issue 1, pp. 10-17.

[40]. Patra, K. C, Kar, N. (2022) 'Suppression Limit cycles in 2 x 2 nonlinear systems with memory type nonlinearities', *International*

Journal of Dynamics and Control, Springer Nature',34, vol.10 Issue 3, pp 721-733.

[41]. Iurashev, D., Campa. G., Anishimov V. V. and Cosatto, E. (2017) 'Three step approach for prediction of limit cycles pressure oscillations in combustion chambers of gas turbines', Taylor and Francis, *Combustion Theory and Modelling*, 21(6), 1-28.

[42]. Tsay, T.S. (2012) 'Stability Analysis of Nonlinear Multivariable feedback Control systems', *WSEAS Transactions on systems*, Volume 11, Issue 4, pp. 140 – 151.

[43]. Tripathy, S.C., Hop, G.S. and Malik, O. P. (1982) 'Optimisation of Load-frequency control parameters for power system with read steam turbines and governor dead band nonlinearity', PROC IEE, Ptc. 129(1), 10-16.

[44]. Patra, K.C., Patnaik, A. (2023) 'Possibility of Quenching of Limit Cycles in Multivariable nonlinear systems with special attention to 3 x 3 systems', WSEAS Transactions on Systems and Control, Vol. 18.

[45]. Oldenburger, R., Sridhar, R., "Signal Stabilization of a Control System with Random Input" *Institute of Electrical Engineers. Part II: Applications and Industry*; Vol.80, Issue 5, 1961, pp 260-268

[46]. Patra, K.C., Patnaik, A. (2023) 'Investigation of the Existence of Limit Cycles in Multi Variable Nonlinear Systems with Special Attention to 3x3 Systems', *Int. Journal of Applied Mathematics, Computational Science and System Engineering*, Vol. *5*, pp. 93-114.

[47]. Sridhar, R., Oldenburger, R. (1962) 'Stability of a Nonlinear feedback system in the presence of Gaussian Noise', *Journal of Basic Engineering*, 84, pp. 61-70.

[48]. Gibson, J. E., Sridhar, R., (1964) 'The Response of Nonlinear closed-loop Systems to Random Inputs', ASME Trans., *Journal of Basic Engineering*, pp. 132-138.

[49]. Ogata K, Modern control engineering, 5th Edn. P H I Learning, pp.723-724 and 2012.

[50]. Raymond, T, et al. (2002) '*Design of Feedback Control Systems'*, Oxford University Press, 4th edition, pp. 677-678

[51]. Singh, Y.P., Some aspects of forced oscillations of non-linear systems (Doctoral dissertation, Ph.D. Thesis, Electrical Engg. IIT Kharagpur, India (1968).

Contribution of Individual Authors to the Creation of a Scientific Article (Ghostwriting Policy)

The authors equally contributed in the present research, at all stages from the formulation of the problem to the final findings and solution.

Sources of Funding for Research Presented in a Scientific Article or Scientific Article Itself

No funding was received for conducting this study.

Conflict of Interest

The authors have no conflicts of interest to declare that are relevant to the content of this article.

Creative Commons Attribution License 4.0 (Attribution 4.0 International, CC BY 4.0)

This article is published under the terms of the Creative Commons Attribution License 4.0
https://creativecommons.org/licenses/by/4.0/deed.en_US